NUMERICAL AND EXPERIMENTAL CHARACTERIZATION OF MELT POOL IN SELECTIVE LASER MELTING OF SS316L

Author

AHSAN KHAN

Registration Number

330607

Supervisor

DR SYED HUSSAIN MRAN JAFFERY

DEPARTMENT DESIGN AND MANUFACTURING ENGINEERING

SCHOOL OF MECHANICAL & MANUFACTURING ENGINEERING

NATIONAL UNIVERSITY OF SCIENCES AND TECHNOLOGY

ISLAMABAD

MARCH, 2023

Numerical and Experimental Characterization of Melt Pool in Selective Laser Melting of SS316L

Author

AHSAN KHAN

Registration Number

330607

A thesis submitted in partial fulfilment of the requirements for the degree of

MS Design and Manufacturing Engineering

Thesis Supervisor:

DR SYED HUSSAINMRAN JAFFERY

Thesis Supervisor's Signature: _____

DEPARTMENT DESIGN AND MANUFACTURING ENGINEERING
SCHOOL OF MECHANICAL & MANUFACTURING ENGINEERING
NATIONAL UNIVERSITY OF SCIENCES AND TECHNOLOGY,
ISLAMABAD

MARCH, 2023

Declaration

I certify that this research work titled *"Numerical and Experimental Characterisation Melt Pool in Selective Laser Melting of SS316L"*s my own work. The work has not been presented elsewhere for assessment. The material that has been used from other sources it has been properly acknowledged / referred.

Signature of Student

NUST-MS-DME-SMME-2023

Plagiarism Certificate (Turnitin Report)

This thesis has been checked for Plagiarism. Turnitin report endorsed by Supervisor is attached.

Signature of Student

Registration Number

330607

Signature of Supervisor

Copyright Statement

- Copyright in text of this thesis rests with the student author. Copies (by any process) either in full, or of extracts, may be made only in accordance with instructions given by the author and lodged in the Library of NUST School of Mechanical & Manufacturing Engineering (SMME). Details may be obtained by the Librarian. This page must form part of any such copies made. Further copies (by any process) may not be made without the permission (in writing) of the author.

- The ownership of any intellectual property rights which may be described in this thesis is vested in NUST School of Mechanical & Manufacturing Engineering, subject to any prior agreement to the contrary, and may not be made available for use by third parties without the written permission of the SMME, which will prescribe the terms and conditions of any such agreement.

- Further information on the conditions under which disclosures and exploitation may take place is available from the Library of NUST School of Mechanical & Manufacturing Engineering, Islamabad.

Acknowledgements

I am thankful to my Creator Allah Subhana-Watala to have guided me throughout this work at every step and for every new thought which You setup in my mind to improve it. Indeed, I could have done nothing without Your priceless help and guidance. Whosoever helped me throughout the course of my thesis, whether my parents or any other individual was Your will, so indeed none be worthy of praise but You.

I am profusely thankful to my beloved parents who raised me when I was not capable of walking and continued to support me throughout in every department of my life.

I would also like to express special thanks to my Supervisor, Dr Syed Hussain Imran Jaffery for his help throughout my thesis and also for Material Selection and Design course, which he has taught me. I can safely say that I haven't learned any other engineering subject in such depth than the one which he has taught.

I would also like to pay special thanks to Mr Syed Zahid Hussain and My Masters fellow, Mr Shakeel Dilawar, for their tremendous support and cooperation. Each time I got stuck in something; they came up with a solution. Without their help, I wouldn’t have been able to complete my thesis. I appreciate their patience and guidance throughout the whole dissertation.

I would also like to thank my Dr Shahid Irkam Ullah Butt, Dr Muhammad Salman Khan, and Mr Syed Zahid Hussain for being on my thesis guidance and evaluation committee and express my special thanks to my Supervisor, Dr Syed Hussain Imran Jaffery for his help.

Finally, I would like to express my gratitude to all the individuals who have rendered valuable assistance to my study.

Dedicated to my exceptional parents and adored siblings whose tremendous support and cooperation led me to this wonderful accomplishment.

Abstract

The additive manufacturing technology Selective laser melting (SLM) also referred as laser powder bed fusion (LPBF) is a technique that can produce intricate metallic parts in 3D. However, maintaining an accurate surface finish and shape can be difficult because of the dynamic thermal cycles of melting and solidification. To produce high-quality products, it is essential to maintain the dynamic stability of melt pool in SLM. This requires studying the temperature distribution and thermal behaviour within the pool. In this study, a Finite Element Modelling (FEM) approach that was experimentally verified was utilized to precisely ascertain the thermal profiles and dimensions of the molten pool. To investigate the impact of different process variables on the shape of the pool during the selective laser melting (SLM) of SS316L powder, a transient model was employed. A FEM model was proposed to evaluate the temperature gradient and characteristics of the molten pool during SLM, with laser penetration depth also taken into account. The proposed heat source model was calibrated with data from the literature. The FEM model was subsequently adjusted and validated through further experimentation to ensure that it accurately predicts the melt pool dimensions and temperature profiles. The model findings were consistent with the experimental data, and the effects of interlayer and intertrack were examined. For each layer and track, the molten pool depth, width, and length of the and the temperature distribution were assessed, and the findings were analyzed for each variable. The FEM model had relative errors of 1.88%, 1.49%, and 2.12% for the predicted melt pool length, width, and depth, respectively, compared to the experimental measurements, for a range of optimal parameters.

KEYWORDS: *Additive Manufacturing (AM), Selective laser melting (SLM), 3D Printing, Finite Element Modelling (FEM), Melt-pool, 3D Gaussian Heat Source, Thermal modelling, SS316L.*

Table of Contents

List of Figures

List of Tables

Chapter 1 Introduction

1.1 Overview:

Additive manufacturing (AM) is a cutting-edge technique that holds significant potential in the fourth industrial revolution. It accounts for the production of 3D metallic components with greater precision and longer production cycles than traditional manufacturing methods. Due to its numerous benefits, additive manufacturing has become a crucial process across various industries. Over past twenty years, additive manufacturing (AM) has made rapid advancements from basic 3D printing to robust, quick production systems that can generate parts without requiring additional tools. An important benefit of additive manufacturing (AM) is its capacity to manufacture components that cannot be produced using traditional methods. Unlike traditional manufacturing processes, which face challenges in producing parts with multiple grooves through milling or welding, additive manufacturing is particularly suitable for manufacturing intricate designs with minimal geometric restrictions. Metal additive manufacturing techniques are particularly valuable for manufacturing highly critical parts that necessitate low-volume production and mass customization, especially in the aerospace, automotive, and biotechnology industries, where the 3D-printed parts must meet all customer requirements for all features. Examples of components that have been successfully produced using additive manufacturing include turbine blades, race car parts, and medical implants, with the finished assemblies exhibiting comparable or even superior properties to those produced using conventional methods [1, 2].

1.1.1 Evolution of AM:

Additive manufacturing has made significant progress since its introduction in the 1980s. Originally developed as a rapid prototyping technology, AM has evolved into a production means that is evolving the industries and transforming the perspective of design and produce parts and products. Over the decades, the technology has undergone significant improvements, from advancements in materials and processes to the development of new software and hardware systems. Additionally, the growth of AM has led to the need for standardization to ensure consistent quality and

interoperability between different systems and processes. As AM continues to evolve, it has the potential to revolutionize manufacturing, offering improved performance, increased efficiency, and the ability to produce customized parts. Over the decades, Additive Manufacturing (AM) has undergone a significant evolution, which is given as follows, highlighting the key developments and advancements that have led to its current state as a disruptive technology transforming industries.

1980s: The first patents for AM were filed in the 1980s, and early applications were focused on rapid prototyping. The earliest machines used stereolithography to create parts by curing layers of liquid photopolymer with a laser.

1990s: in the 1990s, AM began to move beyond prototyping and into manufacturing. Selective laser sintering (SLS) and fused deposition modelling (FDM) were introduced, which expanded the range of materials that could be used in AM.

2000s: in the 2000s, AM saw increasing adoption in a variety of industries, including aerospace, medical, and automotive. New materials such as metal powders and ceramics were introduced, and the resolution and accuracy of AM machines continued to improve.

2010s: The 2010s saw a significant increase in the adoption of AM for production, particularly in the aeronautics industry where AM was used to produce complex, lightweight parts. The number of AM machines and materials available also increased, and new techniques such as direct energy deposition and binder jetting were introduced.

2020s: in the current decade, AM continues to evolve and expand its capabilities. AM s being used in new applications such as food and fashion, and new materials such as living tissue and recycled plastics are being developed for use in AM. The ability to produce large-scale parts and the development of automated post-processing techniques are also expanding the potential uses of AM.

1.1.2 Standardization of AM:

Additive manufacturing (AM) standardization has experienced notable progress in recent decades. With increasing adoption of the technology, there is a growing requirement for standardization to ensure uniform quality and interoperability across various systems and processes. Below is an overview of the advent of AM standardization over the period, highlighting the key developments and advancements that have led to the establishment of industry-wide standards for ensuring consistent quality and interoperability between different systems and processes.

1980s: During the 1980s, additive manufacturing (AM) was a relatively new technology and there were no formal standards in place. Companies that developed AM systems used proprietary technology and focused on prototyping.

1990s: in the 1990s, as the use of AM began to grow, the need for standards became more apparent. The (ASTM) published its first standard for AM in 1990, which focused on the testing and characterization of parts produced by stereolithography. This was followed by standards for other AM approaches, i.e., as SLS and FDM.

2000s: During the 2000s, AM became more widely adopted and its use n production applications increased. The (ISO) published its first standard for AM in 2003, which covered the general principles of AM and the requirements for design, material selection, and post-processing. The ASTM also continued to develop new standards, including those for the qualification of AM processes.

2010s: The 2010s saw significant growth in the adoption of AM, particularly in the aerospace and medical industries. As a result, the need for AM standards continued to increase. in 2013, the ASTM published a standard for AM terminology, which helped to establish a common language for the industry. The ISO developed several new standards for AM, including those for machine testing and the qualification of AM processes. Additionally, organizations such as the AM Users Group (AMUG) and the Society of Manufacturing Engineers (SME) began developing standards specific to their industries.

2020s: In the current decade, AM standards continue to evolve as the technology becomes more widely adopted. The ASTM has developed new standards for AM quality management systems and the validation of AM processes. The ISO has published new standards for surface texture measurements and the production of metal powders for AM. Other organizations are also contributing to the development of AM standards, such as the (NIST) in the United States.

Overall, the evolution of AM standardization has been driven by the need to ensure consistent quality and safety across different AM processes and industries. The development of new standards will be critical to the continued growth and adoption of AM, as well as to ensuring the safety, reliability, and quality of AM products and parts.

1.1.2.1 ***The ASTM Standard:***

ASTM international, is one of the most prominent organizations responsible for developing standards in various industries, including Additive Manufacturing (AM). The ASTM F42 committee was established in 2009 and is responsible for developing and maintaining standards for AM.

The ASTM F42 committee has developed numerous standards for AM, covering various aspects of the process, including materials, design, production, post-processing, and quality control. These standards are designed to ensure that parts produced using AM technology meet the required specifications and are safe for use in their intended applications.

One of the most widely used ASTM AM standards is the ASTM F2924 standard, which covers the design of parts produced using PBF technique AM technologies, such as SLS and EBM. This standard provides guidelines for part orientation, minimum feature sizes, and overhang angles, among other design considerations.

Another important ASTM AM standard is the ASTM F3091 standard, which covers the production of parts using directed energy deposition AM approach, such as LMD and EBM. This standard provides guidelines for machine qualification, process validation, and quality control, among other production considerations.

In addition to these standards, the ASTM F42 committee has developed numerous other standards for AM, covering various aspects of the process. These standards are widely adopted by industry and are considered the de facto standard for AM in many applications.

Overall, the ASTM AM standards are a critical component of the current AM standard, providing comprehensive guidelines for various aspects of the AM process. These standards ensure that parts produced using AM technology meet the required specifications and are safe for use in their intended applications.

1.1.3 Applications of Additive Manufacturing:

AM, a cutting-edge technology causing significant changes in the manufacturing industry, should not be viewed as a replacement for traditional manufacturing techniques. Rather, it serves as a supplementary method that enables the production of intricately designed and custom-made parts with exceptional precision and accuracy. This makes it a valuable tool in industries like aerospace, healthcare, and automotive where precision and customization are of utmost importance. Additionally, AM is an eco-friendlier option since it reduces material waste and energy consumption compared to traditional manufacturing methods. While it may not fully substitute traditional manufacturing techniques, AM can significantly enhance the industry and revolutionize the way we design and manufacture parts and products. It is important to leverage the distinct benefits of additive manufacturing, which arise from the digital process and the ability to create complex shapes, in order to validate the higher cost of parts produced through this method. There are many benefits to using AM, but the most significant are:

Improved design capabilities: The capacity to fabricate intricate designs that would be challenging or unfeasible to manufacture using conventional production techniques is a significant advantage of additive manufacturing. This can result in the creation of more inventive and practical products.

Faster prototyping: Since AM is a digital process, it can be faster and more cost-effective to create prototypes and iterate on designs. This can be especially useful n industries where time-to-markets critical.

Reduced waste: Unlike traditional manufacturing methods, which often involve subtractive processes that generate a lot of waste material, AM is an additive process that only uses the material needed for the final product. This can result in significant material savings and environmental benefits.

Customization: AM accounts for producing highly customized parts and products, which can be tailored to the specific needs of individual customers or applications. This can lead to better performance, functionality, and customer satisfaction.

Reduced tooling costs: With traditional manufacturing methods, tooling can be a significant expense. Since AM is a digital process, there's often less need for specialized tooling, which can reduce costs and lead times.

Reduced assembly requirements: Since AM can produce complex parts in a single print, it can reduce the need for assembly and reduce the risk of errors or defects in the final product.

Additionally, AM offers other benefits such as a high material usage rate of over 90%, the ability to produce complex parts made of high melting point materials, and the potential to improve productivity in the manufacturing process chain through increased geometrical design flexibility.

To sum up, AM presents many advantages that can justify the higher cost of its components, and it's possible uses are wide-ranging and varied. AM has the potential to transform the manufacturing sector by delivering better performance, greater efficiency, and the capability to manufacture tailored parts.

1.1.4 Challenges in Additive Manufacturing:

Additive Manufacturing (AM) offers unique advantages over conventional practices for the producing complex, customized parts with more accuracy and precision.

However, the technology also poses several technical challenges that must be overcome to fully realize its potential. Some of the major technical challenges in AM include:

Material properties: The properties of the materials used in AM can be vary from those produced using conventional manufacturing methods. The mechanical properties, surface finish, and durability of parts produced with AM can vary based on the material used, which can impact their performance.

Process control: AM processes can be sensitive to variations in temperature, humidity, and other environmental factors, which can result in affecting the final quality of the finished product. Hence, controlling these factors can be challenging, requiring specialized equipment and expertise.

Part design: The design of parts for AM can be challenging due to the limitations of the technology. Certain geometries, such as overhangs and unsupported features, may be difficult to produce accurately without additional support structures. This can impact the time and cost of production.

Surface finish: AM-fabricated components frequently necessitate post-processing procedures like machining or polishing to attain the intended surface texture and precision. Obtaining the desired surface finish can be arduous, particularly for parts with intricate geometries.

Scaling up: Although AM is an excellent fit for creating intricate and small components, expanding to larger sizes and quantities can present difficulties. The manufacturing of bigger parts may demand larger equipment, increased materials, and extended production durations.

Process speed: Additive manufacturing techniques can operate at a slower speed compared to conventional production methods, especially when producing larger components. This may have an effect on the duration and cost of manufacturing.

Process repeatability: The repeatability of AM processes can be challenging, particularly for parts with complex geometries or large build volumes. This can impact the quality and consistency of parts produced.

In conclusion, while AM offers numerous benefits, it also poses significant technical challenges that must be addressed. Overcoming these challenges will require ongoing research and development, greater standardization and regulation, and the adoption of new materials and processes. With continued investment and innovation, however, AM holds the significant potential to transform the manufacturing industry and offer new possibilities for customization, efficiency, and sustainability.

1.2 Major Metal AM Processes:

AM is a rapidly growing field with various processes that enable the parts production with a high degree of accuracy and complexity. Some of the most common AM processes include Powder Bed Fusion (PBF), which includes Selective laser melting (SLM) and Electron Beam Powder Bed Fusion (EBPBF); Directed Energy Deposition (DED), which includes Laser Metal Deposition (LMD) and Electron Beam Melting (EBM); Binder Jetting (BJ); Material Jetting (MJ), which includes Drop-on-Demand (DOD) and Continuous Jetting (CJ); and Sheet Lamination, which includes Laminated Object Manufacturing (LOM) and Ultrasonic Additive Manufacturing (UAM). Each process has its own advantages and limitations, and the choice of process depends on factors such as the required resolution, surface finish, material properties, and cost. Choosing the appropriate method is crucial to guaranteeing the required standard and efficacy of the end product.

1.2.1 Electron Beam Powder Bed Fusion (EBPBF):

(EBPBF) is an AM technology that employs an electron beam as the heat source to selectively fuse a powder bed layer-by-layer, resulting in the creation of a three-dimensional component. The procedure resembles (SLM), except that a beam of electrons is utilized to melt the metal powder instead of a laser. An electron gun generates the electron beam, which is subsequently directed towards the metal powder layer through an arrangement of electromagnetic lenses. The heat generated by the

electron beam melts the metal powder, which solidifies as it cools, and the process is repeated to build up the desired part layer by layer.

EBPBF presents an advantage in that it can process a diverse array of materials, including refractory metals, high-temperature alloys, and reactive metals that are challenging to process with other AM methods. EBPBF provides an extensive level of command over the process variables, like beam current, beam velocity, and powder feed rate, allowing for accurate regulation of the melt pool and consequently enhancing the quality of the end product. However, the process is relatively slow compared to other AM processes and requires a high vacuum environment to prevent the electron beam from scattering or interacting with the surrounding air molecules. Additionally, the equipment required for EBPBF can be expensive and requires specialized training to operate.

1.2.2 Laser Metal Deposition (LMD)

(LMD) is an AM method that employs a laser to fuse a metal powder or wire feedstock onto a substrate to create a 3D component. This process is occasionally referred to as Directed Energy Deposition (DED) or Laser Engineered Net Shaping (LENS).

In LMD, the laser melts the metal feedstock as it is placed on the substrate. This capability enables the production of intricate shapes and structures with exceptional accuracy and precision. The process is versatile, accommodating a broad spectrum of metals, such as aluminium, titanium, stainless steel, and nickel-based alloys. The components generated by this technique find application in diverse fields, including the aerospace, biomedical, and automotive sectors.

An advantage of LMD is its adaptability to amend or improve pre-existing components by adding material to a specific region. This allows for the restoration of damaged or worn parts without the need for a complete replacement. Additionally, LMD can be used to add material to a part to improve its properties or to create features that were not present in the original design.

However, LMD does have some limitations. it is a relatively slow process compared to other additive manufacturing processes, and the equipment required can be expensive. Furthermore, the quality of the final product can be impacted by factors such as the quality of the metal feedstock and the precision of the deposition process.

1.2.3 Selective laser melting (SLM):

Selective Laser Melting (SLM) is a type of AM technology that enables the production of intricate three-dimensional metallic parts without the requirement of intermediate processing steps and assemblies that are standard in traditional manufacturing methods. SLM is an incredibly accurate method that can fabricate different types of structures and mechanical components, such as intricate porous shapes that are challenging to produce using conventional means. This process comprises melting metal powder layer by layer utilizing a laser beam to construct a three-dimensional object that can be customized with complex designs and shapes. The SLM process typically involves the following steps:

Powder spreading: The build platform is evenly covered with a thin layer of powdered material.

Preheating: The build platform is heated to a temperature slightly below the melting point of the material that will be utilized.

Laser scanning: The laser scans across the powdered material, selectively melting the particles and bonding them to the previous layer.

Platform lowering: The process is then repeated, layer by layer, until the final part is complete, and the build platform is lowered by one layer thickness each time.

SLM has several advantages, such as the capability of creating complex geometries with high precision and accuracy, the ability to utilize a wide range of materials, and the production of high-strength and durable parts. However, the SLM process has certain limitations that need to be addressed, such as the requirement of post-processing to remove any excess powder and enhance the surface finish, and the

possibility of thermal stress and distortion caused by the localized heating and cooling during the process.

Additionally, SLM eliminates the need for costly tooling and reduces lead times, making it a popular manufacturing method for generating complex components with high accuracy and efficiency. As a result, it is extensively utilized in wide range of industries, to manufacture parts with intricate features that cannot be produced by traditional manufacturing techniques [3, 4]. In the SLM process, a tightly focused laser beam with high energy density is utilized to selectively scan a layer of metal powder. This causes the powder particles to be heated and melted by the laser beam before solidifying and fusing with the previous layer. This layer-by-layer process results on a fully functional three-dimensional object, instrument, or prototype. The laser beam's selective scanning ensures that only the desired areas are melted and fused, allowing for the production of intricate designs and geometries with exceptional accuracy and precision. Consequently, the SLM process has widespread applications in various industries, enabling the rapid and efficient creation of complex and high-quality parts and prototypes [5, 6]. By adding layers of material, SLM has a significant advantage over traditional manufacturing methods in the ability to produce complex shapes with high precision and accuracy without the need for additional tooling or assembly. Moreover, the process melts the entire powder bed, leading to parts with high density, often reaching up to 99.9% density, subject to the material properties and process parameters. As a result, this method produces high-quality parts that have broad applications in different industries [7]. Due to its capability of producing intricate and high-precision components, Selective laser melting (SLM) has gained immense popularity as a Powder Bed Fusion (PBF) technology. This technique is widely adopted across diverse industries, including medical, energy, aviation, automotive, and others [8-12].

1.3 Limitations of SLM:

The productivity rates of SLM additive manufacturing processes are typically lower in comparison with traditional production approaches such as casting and forging. This is because the material deposition rates in SLM usually range only between a few

dozen cubic millimetres per hour (mm^3/h) [13]. SLM additive manufacturing is known for its lower productivity rates when compared to traditional manufacturing methods like casting and forging. As a result, it is usually used for small-scale production of intricate components, industries that have relatively lower production and cost, such as aerospace and medical applications, have seen significant growth in the adoption of additive manufacturing methods. However, the cost of raw materials and lower productivity rates have been identified as significant challenges to the adoption of AM in cost-sensitive industries such as automotive, despite the advantages of producing complex shapes with high precision and accuracy without the need for additional tooling or assembly [14]. It is important to recognize that although additive manufacturing currently faces limitations in creating complex structures for large-scale production, there is potential for new economic opportunities within the industry by increasing the production of intricate components. This is because improving part performance can result in higher component value.

The process of SLM, in which metal powder is melted and solidified, follows a cyclical pattern. The complex thermal gradient created during the process can impact various properties of the final components, including their surface, structural, mechanical, and microstructural properties. Thus, there is a possibility of encountering problems like residual stresses, warping, and cracking that may negatively impact the quality and dependability of the final product. Moreover, the SLM process may result in defects, such as surface roughness and porosity, which require further post-processing to obtain the desired surface finish. Overcoming these challenges is essential to fully utilize the potential of SLM technology in industrial applications [15, 16]. Various issues can impact the production of parts using SLM, leading to physical, mechanical, and metallurgical flaws in the finished product. Defects such as surface regularities, excess porosity, and dimensional accuracy, which is also known as "balling," can arise. During the process, mechanical problems like residual stress and insufficient relative density may also occur. Metallurgical defects can result from high temperatures, leading to the loss of critical elements and microstructural problems. To ensure the quality of SLM components, it is crucial to optimize the processing parameters. Neglecting to adjust these parameters can result in defects and other issues since they play a vital role in determining the final product's quality [17]. When using

SLM in various industrial sectors, accurately modelling the heat source and thermal radiation absorption properties of materials is a significant challenge. The modelling and simulation must also consider the heat dissipation and anisotropy of the parts during the process. Moreover, having a comprehensive understanding of the material's behaviour during solidification and phase transition in the SLM process is important [18, 19]. Limitations for SLM arise from the challenges mentioned earlier, including mass production, robustness, repeatability, and product quality. Determining the ideal processing parameters for a new alloy and machine setup is also a time-consuming and expensive process. To tackle these issues, a comprehensive and precise configuration model that considers thermal gradients, process parameters, and solidification variables during SLM can enhance product quality. Additionally, performing a detailed numerical and experimental melt pool analysis important in reducing the defects caused by the complex underlying production system of SLM [20, 21].

1.4 Significance of melt pool in AM:

The melt pool plays a critical role in AM processes, particularly in powder bed fusion techniques such as selective laser melting (SLM) and electron beam melting (EBM). The powder material is melted by a laser or electron beam during the AM process, which creates a molten pool. This pool then solidifies, forming the desired shape layer by layer. Controlling and monitoring the formation of the melt pool is essential during the AM process, as the size, shape, and temperature of the pool influence the quality and properties of the final manufactured part.

Several factors can affect the size and shape of the melt pool, including the power of the laser or electron beam, scanning speed, and the properties of the powder bed. If the melt pool is too large, it can lead to thermal gradients and induced stresses, causing warping or cracking of the part. Conversely, if the size of the melt pool is too small, it may not completely melt the powder, leading to inadequate quality and compromised part properties.

1.4.1 Melt pool control:

Porosity: The formation of porosity is one of the main concerns that can occur if the melt pool is not adequately controlled during SLM. Porosity is a prevalent defect that can occur during the SLM process due to the entrapment of gas bubbles within the melt pool, leading to voids in the final prod. It can reduce the part's strength and ductility, leading to premature failure or deformation. Hence, optimizing the laser parameters, such as power and speed, for the specific material being used during SLM can help control the melt pool and minimize the formation of porosity.

Cracks: Another issue that can arise if the melt pool is not adequately controlled during SLM is the formation of cracks. Cracks occur as a result of thermal stresses and induced residual stresses on the part, which can arise due to uneven cooling and heating rates. If the melt pool is not adequately controlled, it can result in non-uniform cooling and heating rates, leading to residual stresses and cracks. To prevent cracks, the process variables, such as the scan speed, must be optimized to ensure uniform heating and cooling cycles.

Surface finish: Insufficient control of the melt pool can lead to a surface finish that is uneven or rough, potentially impacting the final product's aesthetics and functional properties. A rough surface finish can cause friction and wear, reducing the part's lifespan. To address this issue, researchers are exploring various methods to control the melt pool, including optimizing laser parameters and developing new materials with better surface finish properties.

In conclusion, controlling the melt pool formation is important for ensuring the quality and performance of the final part during SLM. Insufficient control of the melt pool during SLM can lead to defects such as porosity and cracks in the final part, as well as an uneven surface finish. Various methods are being explored by researchers to optimize the laser parameters and develop new materials that can control the melt pool and ensure consistent quality and performance of the final parts to address these issues.

1.4.2 Melt pool evaluation approaches:

Melt pool is a fundamental component of (AM), especially in Selective laser melting (SLM) processes. To ensure the quality and consistency of manufactured parts, it is important to assess and regulate the formation of the melt pool during the manufacturing process. There are several approaches that can be used to evaluate the melt pool in AM, including:

In-situ process monitoring: This approach involves real-time monitoring using sensors such as cameras, pyrometers, and acoustic sensors. It provides detailed analysis about the size, shape, and temperature of the melt pool, and enables precise control over the process parameters.

Computational modelling: Computational modelling involves the application of simulation approaches to model the melt pool behaviour during the AM process. By utilizing this method, it is possible to gain an extensive comprehension of the thermal and fluid dynamics occurring in the molten pool. This knowledge can then be applied to enhance the manufacturing process by fine-tuning the parameters involved and anticipating the final quality of the produced components.

Post-process characterization: This approach involves analysing the physical properties of the finished parts after the AM process is complete. Through the implementation of this method, it is feasible to acquire data regarding the part's characteristics, such as its microstructure, porosity, and defects. These indicators can offer insights into the efficiency of the melt pool control during the manufacturing process and shed light on the final quality of the product.

In general, a combination of these techniques can be employed to assess the melt pool in additive manufacturing and guarantee that the produced parts meet the desired standards of quality and uniformity.

1.5 Objective:

The aim of this dissertation is to decrease and quantify the variability of SLM components. To achieve this objective, it is essential to have a comprehensive

understanding and control of the thermal evolution of the production process since it is the foundation for minimizing fluctuations in physical characteristics. Once the thermal history is determined using process parameters, it is possible to examine the relationship between the microstructure and features.

Various techniques can be employed to analyse the thermal evolution of SLM components. One commonly used method is experimental measurement during the production process, where thermocouples are utilized to record temperatures simultaneously at different locations. However, measuring temperatures inside the melt pool with thermocouples can be challenging due to high temperatures and gradients affecting measurement accuracy. Non-contact methods are also available for temperature monitoring, but generating the thermal history of a component using a rapidly moving laser and a limited affected area poses its own set of challenges.

Several investigations [22-26] have been conducted to explore the experimental and numerical methods used for ascertaining the thermal history of metal-based powders in additive manufacturing. The Finite Element Method (FEM) is a numerical simulation technique that is extensively used to replicate the thermal evolution and mechanical characteristics of components produced using SLM. This approach can replace experimental measurements by dividing the geometry of the component into small interconnected elements, allowing for a more detailed analysis of temperature gradients, deformation, and stress. The utilization of FEM can facilitate the detection of regions with elevated levels of stress or deformation and contribute to the optimization of process parameters to attain the targeted microstructure and mechanical characteristics of the end-product. However, the accuracy of the results obtained from FEM models is primarily dependent on the precision of the input parameters and assumptions used during the modelling process. Achieving this level of accuracy requires considerable expertise and experience [27]. When a detailed analysis of microstructure modelling is required, Phase-field (PF) simulation can be applied to predict the microstructure's development in SLM. This technique involves solving partial differential equations that describe the progress of a phase-field variable, indicating the local composition and/or order parameter of the material. PF simulation is capable of offering a comprehensive analysis of the morphology,

arrangement, and composition of distinct phases within the microstructure. Furthermore, it can provide valuable understanding into the impact of diverse process parameters on the progression of the microstructure. [28, 29]. To analyse the impact of various process parameters on microstructure during SLM, a macro-scale simulation was conducted using a thermal model based on FEM analysis. The study recognized the significance of thermal evolution in determining microstructure and emphasized the need for a robust thermal simulation system that can be validated across different scenarios.

1.6 Motivation:

In order to advance research in the field of AM, it is important to acknowledge the advantages of utilizing this technique in industry. Selective laser melting is a cost-effective, efficient, and adaptable method for producing parts with complex geometries and precise dimensions. By comprehending the characteristics of the melt pool, the printing process can be optimized to produce high-quality, uniform, and repeatable parts, while avoiding issues such as porosity, recast layers, and distortion. A critical aspect of this research is to comprehend and quantify the significance of different parameters. This understanding is vital for enhancing the printing process and fabricating parts with the desired quality. Furthermore, research in this area is also driven by the potential to create new materials and processes. Selective laser melting can produce parts from various materials, including alloys, polymers, and ceramic composites. By understanding the impact of different parameters on the melt pool, new materials and processes can be developed that result in parts with improved performance and new functionalities.

1.7 Relevance to the national needs:

To produce high-quality and consistent stainless steel 316L components using (SLM), it is essential to understand the characteristics of the melt pool formed during the process. This can be achieved through both experimental and numerical evaluation of the melt pool. Numerical characterization has the potential to facilitate the optimization of process parameters and minimize the occurrence of defects, whereas

experimental characterization can authenticate numerical simulations and enhance the manufacturing process even further. These improvements can lead to the expansion of SLM utilization in industries such as medical, aerospace, automotive, and energy, resulting in more affordable components and wider availability. SLM has advanced in popularity due to its ability to manufacture intricate components with high precision and good surface finish. However, the production of high-quality and consistent parts requires an understanding of the melt pool's characteristics. By characterizing the melt pool through experiments and numerical simulations, the process's physics can be better understood, and the impact of different process parameters can be predicted. This knowledge can help in optimizing the process and reducing the likelihood of defects, making SLM more accessible to industries that require high-quality components. With reduced fabrication costs and time, this technology can become more affordable and widespread.

1.8 Research Significance:

Conducting a thorough analysis of the melt pool in SS316L SLM through both numerical and experimental methods holds significant scientific value. Such an analysis provides valuable insights into the underlying mechanisms of this innovative manufacturing technology. Acquiring an understanding of the distinct features of the melt pool, such as its temperature, size, and dynamics, can assist researchers in comprehending the mechanics of Selective Laser Melting (SLM) and refining the manufacturing process. With this knowledge, the process can become more efficient and accurate, producing high-quality parts in less time. Moreover, this knowledge can facilitate the development of advanced materials for SLM, allowing for the creation of intricate and complex parts. Such advancements are of significant scientific importance and can contribute to the broader progress of advanced manufacturing technologies.

Chapter 2 Literature Review

Significant research efforts, employing both numerical and experimental methods, have been conducted to investigate the thermal behaviour, solidification parameters, and melt pool characteristics in components manufactured through Selective Laser Melting (SLM). These inquiries have made significant contributions to the examination of the laser melting process in SLM, with a primary objective of minimizing defects and enhancing the properties of the fabricated components. In their research, Liu, et al. [30] performed an experimental analysis to study the effect of scan speed on the surface properties of parts fabricated using SLM . Yadroitsev, et al. [31] performed a series of experiments with the objective of determining the deal laser power and scanning velocity for two types of steel, namely SS316L and H13, using SLM technology. By conducting these experiments, the researchers were able to identify the most effective combination of laser power and scanning velocity. A study was conducted by Kusuma, et al. [32] to examine the impact of laser power and scanning speed on the morphology of the molten pool in SLM-fabricated titanium components. The aim of the research was to comprehend the influence of the process parameters on the size and shape of the melt pool. By comprehending the relationship between laser power and scanning velocity, the researchers aimed to optimize the process for producing high-quality titanium parts. The study obtained valuable insights into the influence of different process parameters on the characteristics of the melt pool. Gusarov, et al. [33] examined the melt pool dimensions at high-speed processing using SLM. By utilizing a laser power range of 330-350 W and a scanning speed of 1140 mm/s, the researchers were able to achieve an error value of only 4.16% and 3.94% in the width and depth of the melt pool, respectively. Childs, et al. [34] focused on the influence of process parameters on melt pool across different layers n SLM . They discovered that the powder melting rate was in direct proportion to the scanning speed, concluding that an increase in scanning speed led to an increase in the melting rate of the powder. in their study, Grossmann, et al. [35] evaluated the characteristics of the melt pool and the relative density of titanium alloy lattice structures fabricated using SLM technology. Yasa, et al. [36] conducted a study to

evaluate the effect of re-melting, on the relative density and surface quality of SLM - fabricated components made of Titanium alloy low carbon stainless steel. The objective of the research was to provide valuable insights into the influence of re-melting on the final characteristics of printed geometries. Similarly, Shi, et al. [37] aimed to optimize the processing parameters for the fabrication of Titanium components using SLM by implementing a singletrack numerical approach. They developed the model to predict the characteristics of melt pool and to guide the selection of optimal process variables, which can enhance the accuracy and efficiency of SLM. To validate the model's accuracy, they compared its predictions to previously published experimental results, and the results confirmed that the model accurately predicted the dimensions of melt pool and thermal distribution during the SLM process. This verification step provided substantial evidence to support the use of the model in optimizing the processing parameters for Ti-47Al-2Cr-2Nb SLM components. Similarly, Zaeh and Branner [38] conducted experiments to investigate the significance of powder layer thickness on the deformation of SLM parts, with a particular focus on thin layers that are prone to distortions due to temperature changes. The researchers aimed to determine how different process variables, such as powder layer thickness, scanning patterns, and initial base plate temperatures, could affect the deformation of cantilever shapes in the SLM process. The investigation revealed that the initial temperature of the base plate exerted a substantial impact on the deformation of the cantilever shape, with greater initial temperatures producing more notable deformations. Conversely, the scanning pattern and layer thickness exhibited minimal effects on deformation, where a layer thickness of 75 µm resulted in lower deformations. The researchers stressed the significance of implementing comprehensive layer-based models to precisely anticipate residual stresses and deformations in components produced using SLM.

Due to the complexity of SLM, which involves localized heating using lasers, rapid melting, and solidification, conducting experimental analysis can be challenging. As a result, computational modelling has become an essential approach for understanding the subordinate mechanisms of SLM system. The Finite Element Method (FEM) is a commonly employed numerical technique in predicting temperature and stress profiles during the SLM process. Recently, researchers have been utilizing FEM to analyse

temperature profiles and stress evolution during the SLM process, and to evaluate the impact of processing parameters on product quality. Different simulation scales use the mesoscale approach, which considers the distribution of individual powder particles, and the macroscale analysis, which examines the entire component design. These models aid in determining the most favourable SLM process variables. Leitz, et al. [39] conducted a simulations-based study using a Multiphysics model to investigate the effect of laser power on melt pool dimensions in molybdenum and steel. The primary goal of the investigation was to examine the width of the melt pool. The researchers observed that the width of the melt pool was broader in steel than in molybdenum. Similarly, Huang, et al. [3] utilized a simulation model to conduct a computational analysis of a single-layer, single-track SLM process for a titanium alloy (Ti6Al4V) using evaporation and power absorption. This analysis was carried for a subsequent investigation of thermal profile. Similarly, Zhang, et al. [40] proposed a model that incorporates the fluid flow and heat transfer to investigate about the effects of process variables on thermal gradient within a melt pool of SS31L during SLM. Li, et al. [41] evaluated an (FEM) model based on a single-layer, multiple-track approach to analyse temperature and stress distributions within thin-walled geometries produced through SLM. In addition, they developed a numerical model consisting of two layers to examine how the solidification behaviour of a Titanium alloy s affected by scanning patterns. Similarly, Matsumoto, et al. [42] utilized finite element analysis (FEA) to analyse the thermal behaviour of single-layer powder-based parts produced through SLM. The researchers developed a comprehensive model that couples MATLAB and ANSYS FEM models, enabling the investigation of a non-linear model with a volumetric heat source. Similarly, Luo and Zhao [43] optimized their simulation model in terms of computational cost. This approach enables a more accurate and efficient analysis of the thermal behaviour of parts during the SLM process, and the researchers achieved impressive results with only 2.32% and 7.10% relative errors n melt pool width and depth, respectively. Also, Ma and Bin [44] suggested an FE model for simulating the laser deposition process, utilizing finite element analysis (FEA) modelling. Similarly, Nickel, et al. [45] proposed a study by examining the effect of layer deposition pattern orientation on component stresses and deflections. Their findings highlighted the significant impact of the layer deposition pattern orientation on the produced component's resulting stresses and deflections. To investigate this

phenomenon, the researchers used a moving mesh and weak constraints approach. This technique accurately represents the actual SLM process by accounting for the dynamic changes in geometry and heat transfer throughout the process. Moreover, the use of weak constraints provided a more realistic representation of the material behaviour, accounting for the material's non-linear and anisotropic nature. Artinov, et al. [46] proposed a Multiphysics approach in order to predict the thermal characteristics during laser welding. A novel three dimensional mesoscopic mode was developed by Khairallah, et al. [47] that couples thermal diffusion and hydrodynamics in order to simulate the complex dynamics of metal powder melting and solidification n the powder bed fusion (PBF) process. The mesoscopic model takes into account the microscale phenomena that occur during the melting and solidification of metal powders, such as the powder bed morphology, particle size distribution, and powder layer thickness. The researchers were able to investigate the impact of process parameters on the melting and solidification behaviour of metal powders by simulating these microscale phenomena. The ALE3D multiphase code and finite volume formulation used in the model provides an accurate representation of the fluid dynamics and heat transfer throughout the melting and solidification of metal powders. The model predicts the temperature distribution, thermal gradients, and solidification front movement within the melt pool, as well as the powder particle motion and distribution during the PBF process. Yan, et al. [48] designed a comprehensive Multiphysics 3D model to investigate the SLM process at the powder-scale. Their model integrated the powder flow, heat transfer, melting, and solidification processes, providing a more comprehensive analysis of the SLM process. The researchers highlighted the effectiveness of a continuum-based finite element method (FEM) n modelling SLM, and its potential to improve the understanding of the complex interplay of physical phenomena involved in the process. The approach taken by Yan and his team has significant implications for accurately predicting and controlling the fabricated parts properties in the context of SLM modelling. in order to study the (SLM) process, Foroozmehr, et al. [49] developed a 3D FEM by incorporating the optical penetration depth (OPD) of the laser beam into the metal powder, the model provides a more accurate representation of the heat transfer process during laser melting.

The developed model has the potential to contribute significantly to the optimization of the SLM process by accurately predicting the melt pool dynamics and resulting microstructure of the fabricated parts. Similarly, Yin, et al. [50], Ibraheem, et al. [51], Shuai, et al. [52] used the element birth and death method to analyse thermal gradients n single metallic layer SLM processes. This technique, which utilizes finite element analysis, allows for the creation and removal of finite elements to capture the dynamic changes in the melt pool's geometry. They utilized this approach to simulate the temperature field and thermal stress distribution during SLM and discovered that the thermal gradient in the melt pool was substantial, resulting n a significant temperature difference between the top and bottom of the melt pool. Additionally, they also utilized the element birth and death technique to examine how various scanning strategies affect thermal gradients in the SLM process.

Upon reviewing past studies on SLM modelling, it became apparent that the majority of research focused on idealized geometric models, which did not consider real time SLM phenomenon. Although these models illustrated how thermal behaviour correlates to the shape of the melt pool, they lacked practical relevance because actual production processes involve multi-track, multi-layer SLM. Additionally, the temperature profile of this process can vary significantly from that of single-layer or single-track models. Single-track multi-layer models are also unable to accurately assess the impact of layer count on temperature variables in a multi-layer multi-track process. Only a limited number of studies have investigated thermal simulations or experiments on multi-track, multi-layer models, particularly for 316L steel.

To bridge this research gap, the proposed study aims to develop a 3-dimensional (FEM) model at the macro scale that accurately represents the SLM process. The model incorporates element birth and death functions and varies process parameters, to analyse changes in thermal behaviour and melt pool dimensions. The developed FEM model is verified with previous literature and experimentally tested by printing various samples using different sets of process parameters to confirm the findings. This study is a significant contribution to the field as it offers a comprehensive simulation approach for multi-track, multi-layer SLM processes and provides new insights into thermal behaviour and melt pool dimensions.

Chapter 3 Methodology

3.1 Process Overview:

The essential components involved in the (SLM) process are highlighted in a schematic overview provided by Figure 3.1. The process commences by utilizing mobile mirrors to direct a high-quality laser beam onto the powder bed. The process is typically conducted at high thermal values ranging from 50-2000°C, which are maintained by setting a specific temperature for the build plate. Additionally, an inert or noble gas is used to fill the chamber during the printing process to prevent parts and powder from oxidizing. To maintain the oxygen content at approximately 0.1%, an oxygen sensor is placed at the top of the machine, which introduces more inert gas when needed to regulate the oxygen content of the processing gas.

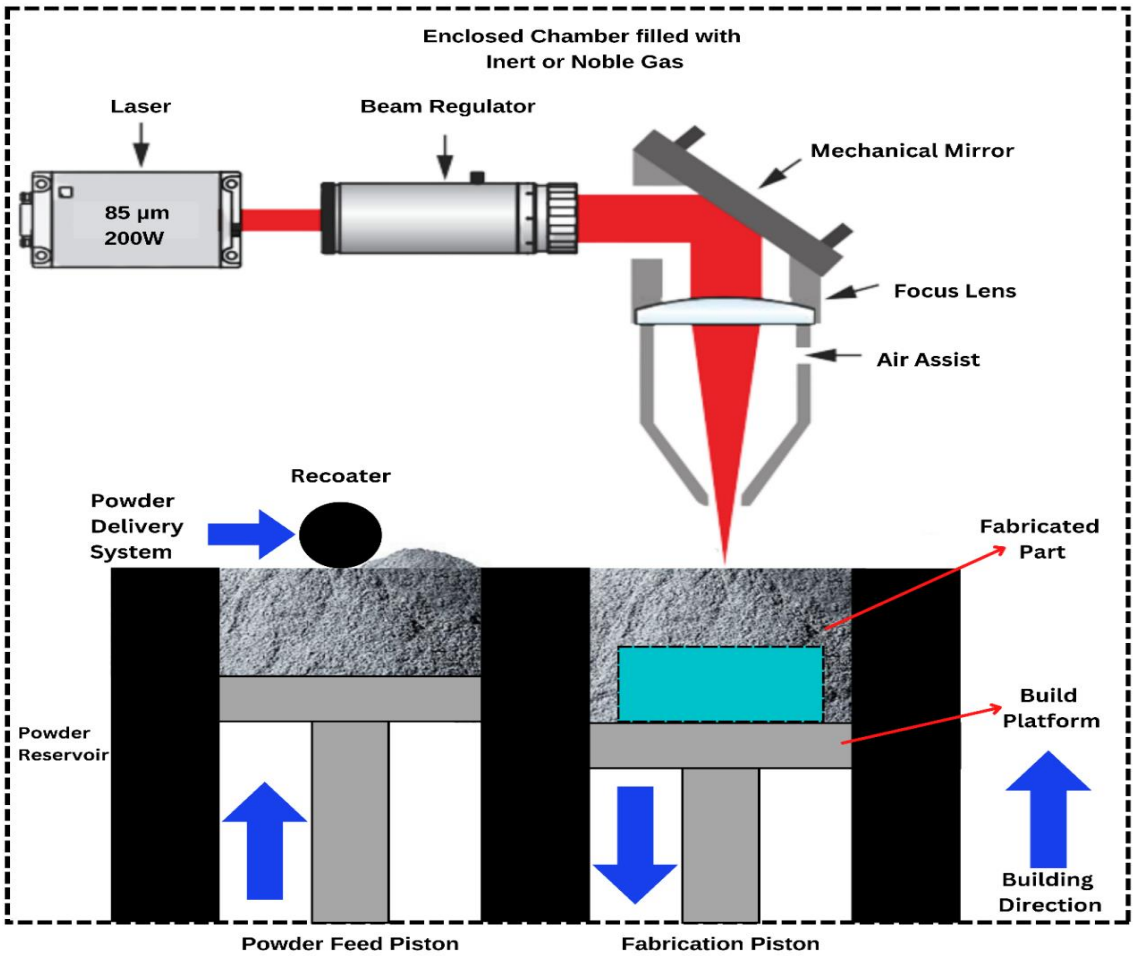

Figure 3.1. Additive Manufacturing Schematic Overview

In (SLM), the recoater blade is a critical component responsible for distributing the powder. The blade's composition can differ based on design specifications, component tolerances, and material type, with steel, ceramic, carbon brush, or rubber being commonly used materials. For optimal results, the powder particles should be spherical with a wide particle size distribution and minimal satellites. High material utilization is possible with SLM, as the unused powder can be collected and reused in future builds.

The integration of cameras and sensors into real-time monitoring systems has revolutionized the observation of the melt pool and powder bed. This integration enables information collection that can be utilised to analyse the impact of different process variables and design characteristics on the final product. Additionally, this data can be utilized to refine parameters and optimize the build process, resulting in improved quality and efficiency.

3.2 Workflow of SLM:

The workflow for SLM can be described as follows n Figure 3.2.

1. The first step in additive manufacturing using SLM involves designing and optimizing a part using a 3D CAD package.

2. Transform the part's CAD model into an STL format that utilizes a triangular representation of the part [53]

3. To prepare the designed part for additive manufacturing, the STL file is imported into dedicated software, i.e., materialize magics. In which, the part is positioned on the build plate, to define its build orientation and add support structures.

4. Export the part and its support structures to a software designed for the specific machine.

5. Transfer the designed part to the AM machine.

6. Load the powder into the machine, adjust the build plate levels, and deposit the first layer of powder onto the build plate

7. After finishing the build, sieve and vacuum the unmelted powder

8. Perform the Manual post-processing following 3D printing, which could include tasks such as collecting the untreated powder, separating the part from the build plate, and taking off support structures.

Subject to part specific application, it may be necessary to employ further post-processing treatments in order to attain the desired surface finish. Such treatments may include various heat treatments as well as abrasive finishing methods such as blasting and polishing.

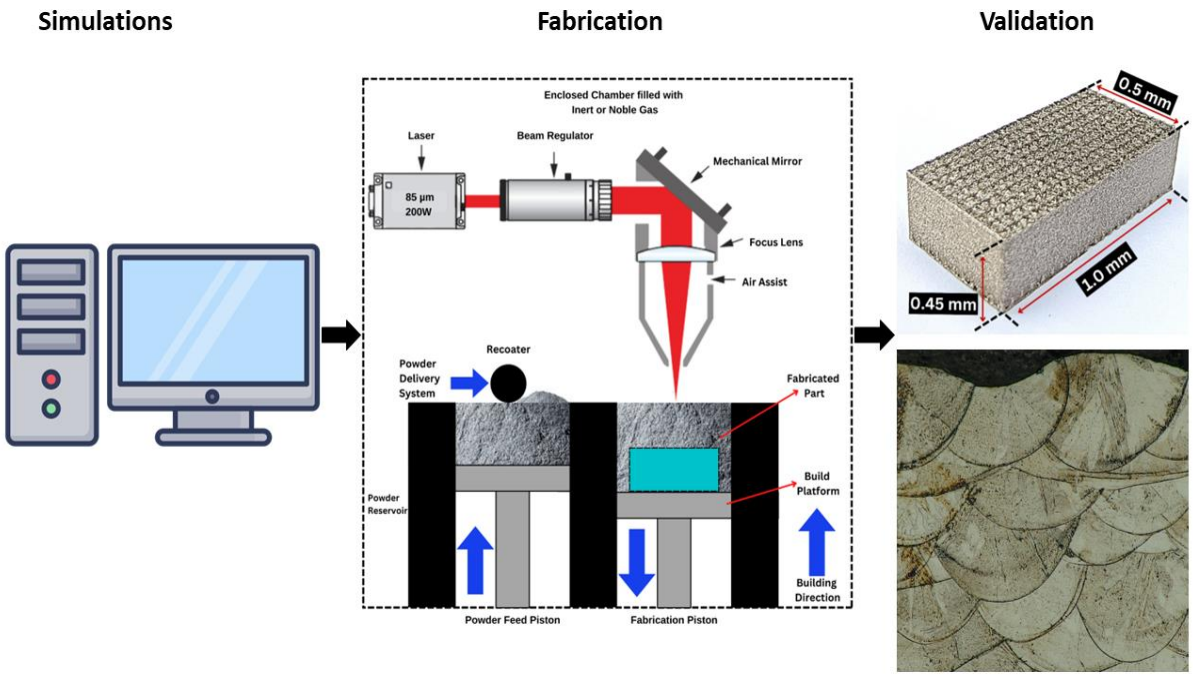

Figure 3.2. Workflow of SLM

According to estimations, as much as 45% of the cost in SLM is attributed to pre- and post-processing activities [54]. However, it is worth mentioning that the cost of SLM can be effectively reduced by creating a design tailored to additive manufacturing. This method eliminates the need to repeat pre-processing operations for each

production cycle of the part. Moreover, if the part is intended for mass production, pre-processing activities will only need to be carried out once. Additionally, optimizing the part's dimensions and orientation during the design phase can decrease the necessity for support structures, further reducing the overall cost of the part. The use of this technique can increase production capacity and justify the high initial investment costs linked with the SLM process.

3.3 Overview of Process Parameters:

Studies have shown that achieving favourable repeatability in the SLM process requires precise control over process parameters and feedstock materials. As a result, several research studies have focused on developing methods to produce lightweight, durable, and accurate parts [55]. These investigations have demonstrated that the laser-related variables such as layer thickness, hatch spacing, scan speed, laser power and beam radius have the most significant impact on the quality of the produced parts [56-60]. The reason why research has primarily focused on developing laser-related parameters might be due to their significant impact on the quality of manufactured parts. This entails evaluating and establishing connections between the parameters and the quality of the product as well as its microstructure. While other parameters such as recoater speed, build plate temperature, and process atmosphere may also be important, they have not received as much attention. The preceding section outlines the primary process parameters and scanning techniques used in SLM.

In SLM, the scan speed refers to the velocity at which the laser beam moves, while the scan vector denotes the direction of the laser beam. It is noteworthy that in some SLM processes, a pulsed laser beam is employed instead of a continuous one, which implies that the time spent at each point is proportional to the scan speed.

The laser beam heats the powder to a temperature higher than its melting point, resulting in the creation of a melt pool. The typical diameter of the laser beam spot is 70-150 μm. The structure of the melt pool from three different angles is illustrated in Figure 3.3 a and b The teardrop shape of the melt pool is observed as it progresses, similar to that seen in welding. It has been demonstrated through research that the size

and shape of the melt pool have a substantial effect on the quantity and type of defects, as well as the microstructure of the resulting parts. [25, 61, 62].

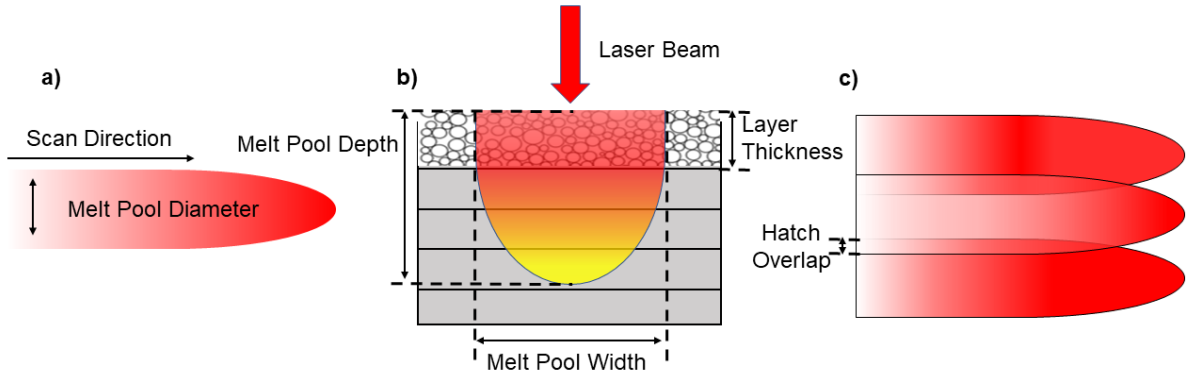

Figure 3.3. SLM Process parameters

To ensure a part that is fully consolidated with minimal defects or lack of fusion, it is crucial to carefully acknowledge the distance coincided scan vectors, or hatch distance, as depicted in Figure 3.3 c. The process involves melting and fusing previously solid layers by manipulating process parameters to allow penetration of 3-5 layers into the previously solidified material. The temperature of the final layer being melted is brought close to its melting point. Subsequently, as new layers of powder are melted, the temperature gradually decreases as the distance from the melt pool increases. This results in an in-situ heat treatment of the built part, triggering diffusion processes that lead to grain growth, phase transformations, and precipitation [26-30]. Additionally, the small interaction volume that results from the rapid heating and cooling, followed by remelting, can create high internal stresses by constraining the surrounding material. After the complete melting of the entire cross-section, the build plate is lowered to compensate for any solidification shrinkage that may have occurred, thereby adjusting the layer thickness as required.

The scan pattern, which determines the path of the scan vector, is critical to achieve the desired fabrication quality. It affects various factors, including the type and amount of defects, microstructure, surface roughness, and residual stresses in the final product [63-67]. In Figure 3.4a, the unidirectional scanning strategy is demonstrated, where the scan vectors move from one side to the other in the same direction in all layers. This is considered the simplest scan strategy. However, it is not commonly used

because it has a tendency to increase the amount of residual stresses in the final product [75]. A faster scanning technique is two directional scanning, which involves reversing the scan vectors when they reach the part boundary, as illustrated in Figure 3.4b. The chess pattern, which is also referred to as island scanning and shown in Figure 3.4c, is a commonly employed scan strategy. This method divides the cross-section into smaller boxes and applies either unidirectional or bidirectional scanning within each box to minimize residual stresses [68].

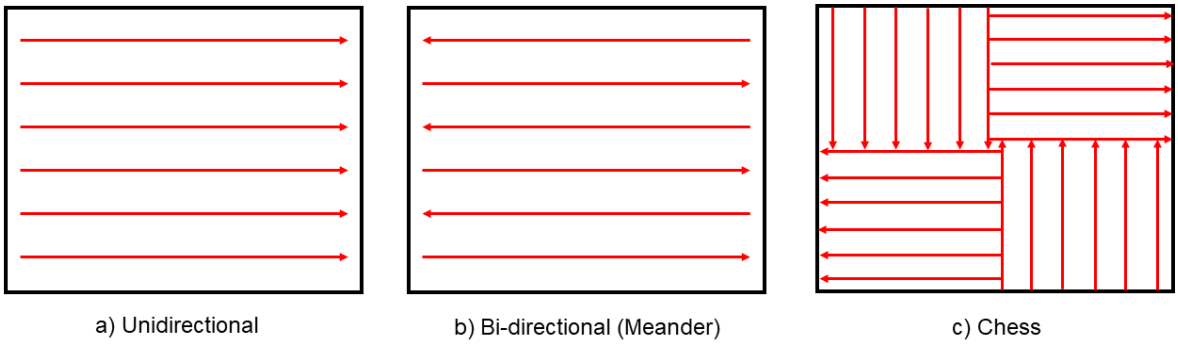

Figure 3.4. Scanning strategies

Scan strategies can be improved by rotating the pattern, as illustrated in Figure 3.5. The angles of the scan vectors or stripe orientations are known as scan rotation angles, and they are adjusted by a certain degree after each layer. A typical scan rotation angle of 67° is often used to achieve the maximum spacing between angles. as explained by J.A. Pakkanen [69]. Although rotation angles like 61° can also provide comparable spacing, most commercially available SLM processes use 67° as their standard rotation angle. Studies have shown that inclining the scan rotation angle can decrease residual stresses, reducing the potential for distortions [69, 70].

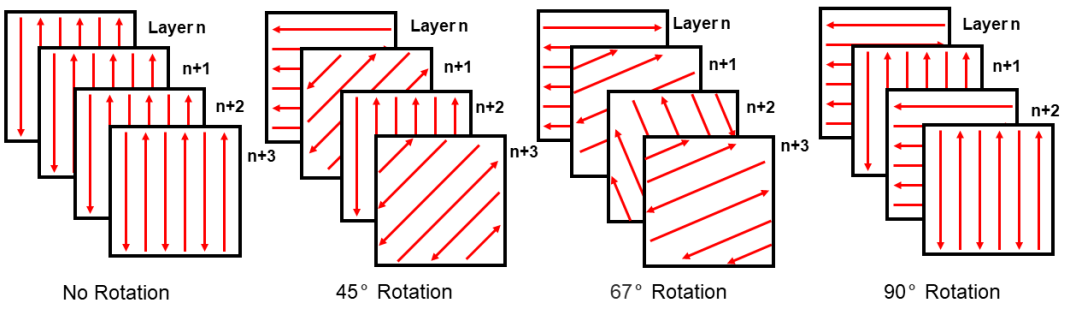

Figure 3.5. Layer-wise hatch rotation

A contour scan is utilized to melt the boundary or outline of the part after melting the whole cross-section, as illustrated in Figure 3.6. The process of contouring, which involves re-melting the outline of the part, can be performed either before or after creating the main cross-sectional area and is carried out to enhance surface quality [71].

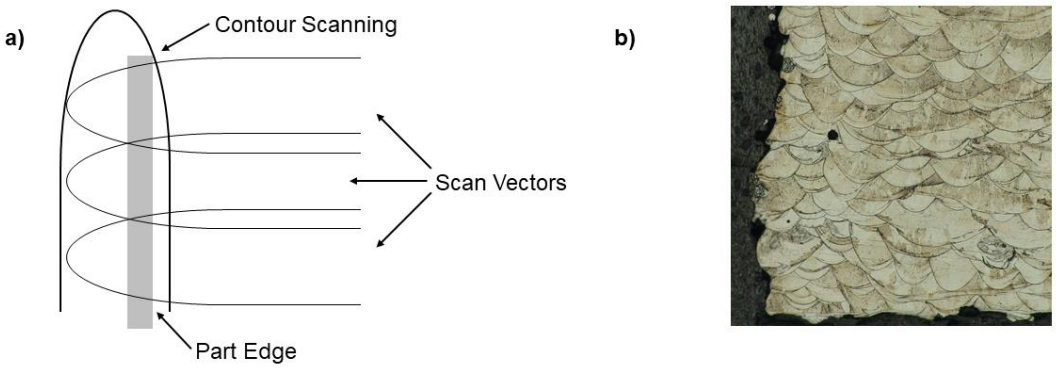

Figure 3.6. Contouring

Employing a protective atmosphere in SLM is crucial to minimize oxidation of both powder and produced parts, as well as to eliminate by-products such as fumes and spatter. The negative consequences of oxidation have been demonstrated to include faulty parts and reduced powder recyclability [71, 72]. To avoid oxidation or nitridation, a gas is introduced into the process chamber to reduce the levels of oxygen and other impurities, including nitrogen. The introduction of gas into the process chamber to lower the concentration of impurities is necessary to prevent diffusion-controlled reactions. As a protective atmosphere, argon gas is commonly used in many SLM processes. However, for materials that are not affected by nitrogen dissolution and nitride formation, nitrogen gas can also be utilized. This is because the rapid

cooling rate in additive manufacturing can lead to the formation of nitrides and the dissolution of nitrogen, which can compromise the properties of some materials [72]. Research has indicated that the utilization of nitrogen, instead of argon, does not affect the microstructure or mechanical characteristics of 316L. Moreover, it is possible to apply gas flow along the entire powder bed to prevent the formation of by-products like spatter, fumes, and projections that occur during the melting process.

3.4 Thermal Modelling:

The equation that governs the 3-dimensional heat transfer is the Fourier series heat equation [56]. This equation is utilised for modelling in various studies [73-76].

$$\frac{\partial}{\partial x}\left(k_x(T)\frac{\partial T}{\partial x}\right) + \frac{\partial}{\partial y}\left(k_y(T)\frac{\partial T}{\partial y}\right) + \frac{\partial}{\partial z}\left(k_z(T)\frac{\partial T}{\partial z}\right) + Q = \rho(T)c(T)\frac{\partial T}{\partial t} \quad (1)$$

In the equation Q accounts for the heat produced/unit volume, while ρ indicates the material density, and c is the specific heat capacity. While, T and t are variables that determine the amount of energy produced per unit volume. Whereas, values k_x, k_y, and k_z represent the thermal conductivities in the x, y, and z directions, respectively.

Assume the powder bed to be isotropic and homogeneous, the above equation (1) can be simplified as

$$k(T)\frac{\partial^2 T}{\partial x^2} + k(T)\frac{\partial^2 T}{\partial y^2} + k(T)\frac{\partial^2 T}{\partial z^2} + Q = \rho(T)C(T_o)\frac{\partial T}{\partial t} \quad (2)$$

where $k(T)$ represents the material's isotropic thermal conductivity. T_o is the ambient temperature, which was 22 °C for the FEM model [56].

The thermal model relies on several underlying assumptions to accurately simulate the heat transfer phenomena occurring during SLM. These assumptions include:

1. The laser moves in traverse direction while material remains stationery.
2. The model does not consider the impact of advection on the material.

3. The heat transfer process is simulated using a constant coefficient, which considers both the losses as a result of convection and radiation.
4. Heat input into the material is modelled by a constant surface absorptivity to represent the material's absorption of laser radiation.
5. The model considers the transfer of heat over time and takes into account the three-dimensional and transient nature of the heat transfer.
6. The assumption is made that the power density is not sufficient enough to cause the SS316L material to evaporate and transition from a solid to a gaseous state.
7. The assumption made in the thermal model is that the material being analyzed has uniform properties in all directions, meaning that it is isotropic.
8. The assumption is made that there is an absence of convection in the liquid pool or at the interface between solid and liquid, and that the material is pure with no mushy region.

3.4.1 Boundary Conditions:

Accurate simulation of laser heat transfer on a metal surface requires careful consideration of multiple boundary conditions that influence the heat transfer mechanisms. When working with lasers, it is essential to consider various factors, including the temperature of the metal surface and the surrounding environment, the duration and intensity of the laser beam, the thermal properties of the material being used, and any cooling mechanisms employed. The efficiency of heat dissipation is determined by the various modes of heat transfer such as conduction, convection, and radiation, which are influenced by these factors [77]. During SLM and other additive manufacturing techniques, conduction is the primary mode of heat transfer, whereas radiation, convection, and evaporation account for a smaller amount of heat transfer. To include radiation in the simulation model, it can be considered as a surface boundary condition. It is essential to note that in SLM (Selective Laser Melting), the laser intensity absorbed by the part is not sufficient to convert it from a solid to a vapor

state; hence, the model does not include an evaporation boundary condition in the heat transfer simulation [47, 78]. The effectiveness of heat transfer is critical in additive manufacturing processes, particularly in SLM, where critical control of the temperature profile is necessary to achieve high-quality prints. The thermal properties of the material used in the printing process, such as thermal conductivity, specific heat, and density, have a considerable impact on the heat transfer mechanisms. The material used and the cooling mechanism employed can affect the heat transfer rate, resulting in varying thermal profiles and ultimately affecting the overall properties of the printed part. Therefore, it is necessary to consider all the boundary conditions in the simulation model to achieve accurate predictions of the thermal profile during SLM [79].

3.4.1.1 Mode of Heat Transfer	*Equation*	
Conduction	$q = -k\nabla T$	(2)
Convection	$q_c = h(T - T_\infty)$	(3)
Radiation	$q_r = \varepsilon\sigma(T^4 - T_\infty^4)$	(4)

The symbol "q" represents the conduction heat rate "k" indicates the material thermal conductivity, q_c denotes convection heat transfer, h represents the convection heat transfer coefficient, q_r indicates rate of radiation heat transfer, ε denotes the material emissivity, σ is the constant of Boltzmann, T_∞ represents the ambient temperature, and T represents the temperature of the medium. The temperature of the room has been assumed to be 22 ℃ in the current study.

3.5 FEM Model:

In the SLM process, accurate simulation results require the provision of an appropriate heat source model. The heat source model describes how the energy is distributed and the thermal profile of the laser beam that is utilized for melting the metal powder. In previous studies, researchers have investigated the use of both 2D and 3D Gaussian distributions to model the heat source. While some studies have argued that 3D modelling provides more accurate results due to its ability to capture the shape of the laser beam more accurately, others have preferred the simpler 2D approach.

The current study employs a macro-scale model that uses a 3D Gaussian heat source to model the laser. This approach is widely used in industry and has been shown to provide precise measurements of the thermal profile of the laser beam and accurate representation of its energy distribution. The volumetric Gaussian heat source model is formulated based on the heat transfer equation, which considers the absorption of energy by the metal powder, as well as the convective and conductive heat transfer between the powder bed and the substrate. The use of a 3D Gaussian heat source model ensures that the laser beam's energy distribution and thermal profile are accurately represented, thereby providing accurate predictions for the SLM.

The following is the governing equation applied for modelling of laser beams is presented below:

$$Q = \frac{2\eta P}{\pi R^2 S} \times e^{\left(\frac{-2(x^2+(y-Vt)^2)}{R^2}\right)} \times e^{\left(\frac{-|Z-nH|}{S}\right)} \quad (9)$$

3.5.1 Python linked with ANSYS:

The 3D Gaussian heat source model applied in this study is composed of two components, namely the applied laser power (a) and the coordinates for laser scanning (b). The coding for the laser trajectory and power supply was implemented using the Python programming language and was subsequently imported into ANSYS. The heat generated by the laser is represented by the term Q in equation (9), while η accounts for the laser absorptivity, R represents the laser radius, V denotes the laser scan speed, S represents the laser penetration depth, P accounts for the laser power, t represents the laser running time, n denotes the number of layers, H represents the layer thickness, and X, Y, and Z denote the coordinate system.

3.5.2 ANSYS Modelling:

To construct a precise and accurate 3D Gaussian Heat Equation-based, a macro scale multi-layer, multi-track finite element model, the researchers utilized the commercial software package ANSYS R21. The model's geometry was carefully designed, with dimensions of 1.0×0.5×0.45 mm³, while the substrate dimensions were set to 2.0×1.0×0.2 mm³ (L×W×T). Figure 3.7. illustrates the geometry built for the model.

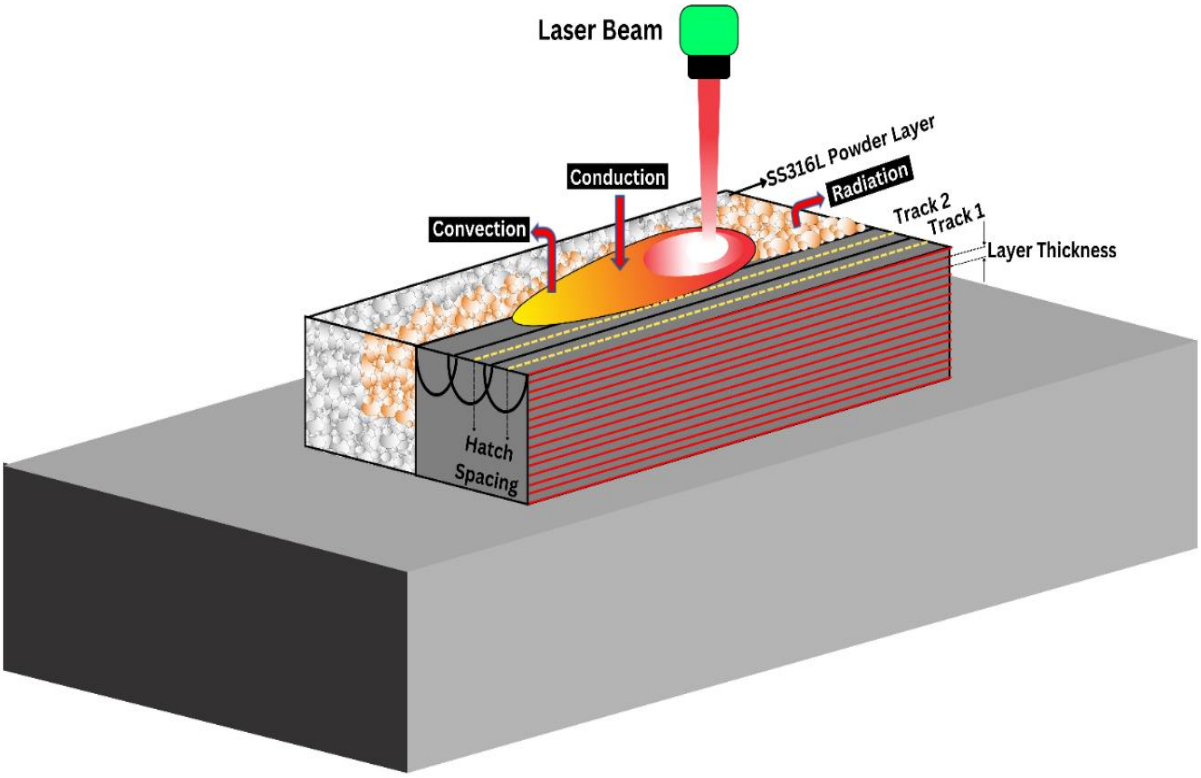

Figure 3.7. Gaussian heat source model overview

A commercial software package ANSYS R21 was due to its ability to provide advanced modelling and simulation capabilities, including the ability to perform complex thermal simulations with high accuracy. The software is widely used in the industry and research fields for FEM analysis and has been proven to be a reliable tool for heat transfer simulations.

The constructed geometry was carefully designed to accurately represent the SLM process and included various features such as the laser beam, powder bed, and substrate. The 3D model was divided into multiple layers, and each layer was further divided into multiple tracks, allowing for a more accurate representation of the complex heat transfer process that occurs during SLM.

The proposed FEM model allowed for the consideration of various factors that affect heat transfer mechanism during the SLM process, such as the duration and intensity of the laser beam, thermal properties of the material used, and cooling mechanisms applied.

3.5.3 Meshing and its significance:

The process of meshing is fundamental to simulation and computational modelling. It involves the division of the computational domain into smaller geometric elements known as "mesh," allowing for the numerical solution of complex mathematical equations. Meshing is typically performed in three stages: pre-processing, processing, and postprocessing.

During pre-processing, the geometry of the object is imported into the simulation software and refined to create a clean model. The mesh is then generated by dividing the model into smaller components. The size of the mesh elements is critical for achieving accurate simulation results. The element size should be optimised enough to capture the geometry's features but not so small that it requires excessive computational resources.

In the processing stage, the simulation is executed using the mesh created in the pre-processing stage. The equations governing the system's behaviour are solved numerically, and the results are obtained. The quality of the results is determined by the accuracy of the mesh, and a poorly generated mesh can lead to erroneous or misleading outcomes.

During the postprocessing stage, the simulation findings are scrutinized and visualized. This process entails generating plots, graphs, and animations to investigate how the system behaves under different circumstances. The data obtained is then analyzed to arrive at well-informed conclusions.

In conclusion, meshing is an integral component of simulation and computational modelling, allowing for the precise and efficient solution of intricate mathematical equations while providing insights into the system's behaviour. The precision of the simulation results is significantly reliant on the mesh's quality, as a well-constructed mesh is crucial for producing reliable and meaningful outcomes.

3.5.4 Mesh Generation:

To ensure accurate measurements of temperature gradients and melt pool dimensions, the constructed part underwent meticulous meshing. A fine mesh configuration was used, while a coarse mesh configuration was applied to the base plate to minimize computation time. The process is illustrated in Figure 3.8. for better understanding. The mesh element size was determined based on established literature that has been published and verified, which states that the mesh size should be equivalent to the half of the deposited material layer in the build direction (Z-axis) and half of the hatch spacing in the scan track (Y-axis) [30, 80]. This helps to ensure that the simulation accurately captures the details of the part's geometry.

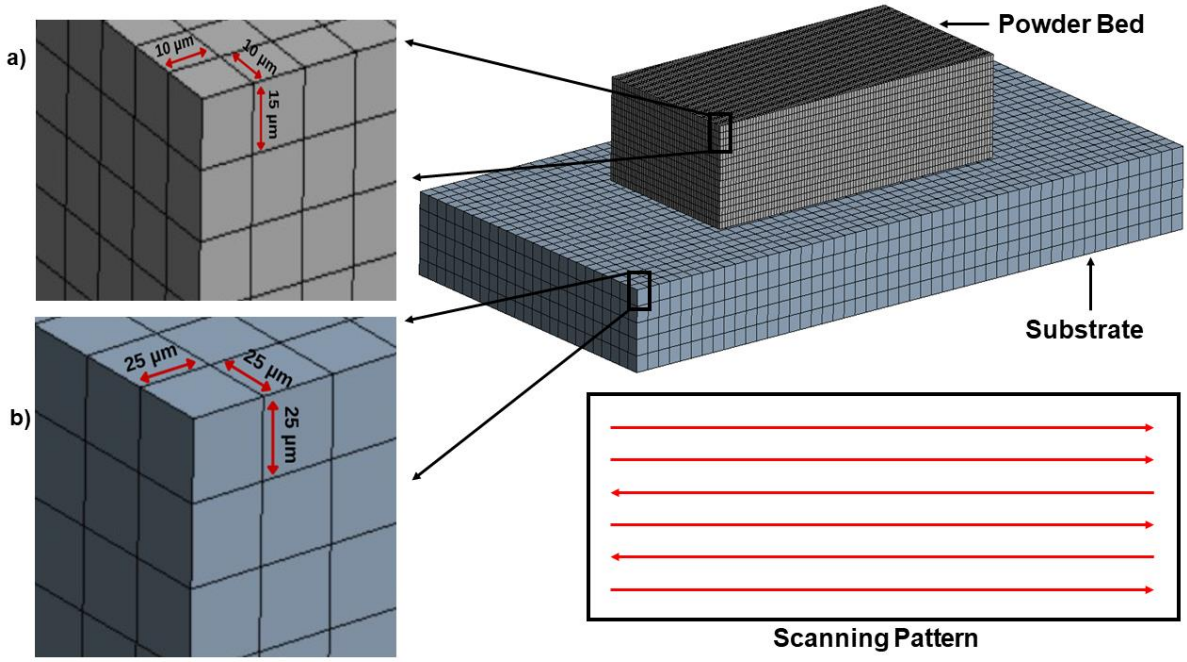

Figure 3.8. Meshing and scanning strategy

To analyse the properties of the molten pool across 15 layers and 6 tracks, a two directional (meander) scanning technique was used for each subsequent track. This technique replicates the material birth and death function as observed in the real SLM process [81]. The use of this technique enables the simulation to accurately capture the complex dynamics of the laser-powder interaction during the printing process, providing accurate results.

Similarly, Table 3.3. Includes other variables such as hatch spacing, laser beam radius, laser power, and scan velocity, in addition to deposition of a constant powder layer thickness of 30.0 µm for receding layer deposition. The part is built along the Z-axis, laser moves along the Y-axis to scan the powder. The intertrack and interlayers delay times are established at 2.0 sec and 10.0 sec, respectively. These variables were chosen to ensure that the simulation accurately captures the dynamics of the printing process and provides precise measurements of temperature gradients and melt pool dimensions.

3.5.5 Model`s Mesh and Time Step independence:

The objective of the grid independence analysis in this study was to determine the most appropriate grid size and time step for the model to achieve precise simulation results. The process involved the use of three different mesh configurations, consisting of 65,000, 94,000, and 159,000 grid elements, each with varying time steps of 2, 3, 4, and 5 µsec, as illustrated in Figure 3.9. The goal was to select a mesh configuration and time step that did not affect the dimensions of the melt pool, such as length, width, and depth, and provided accurate results.

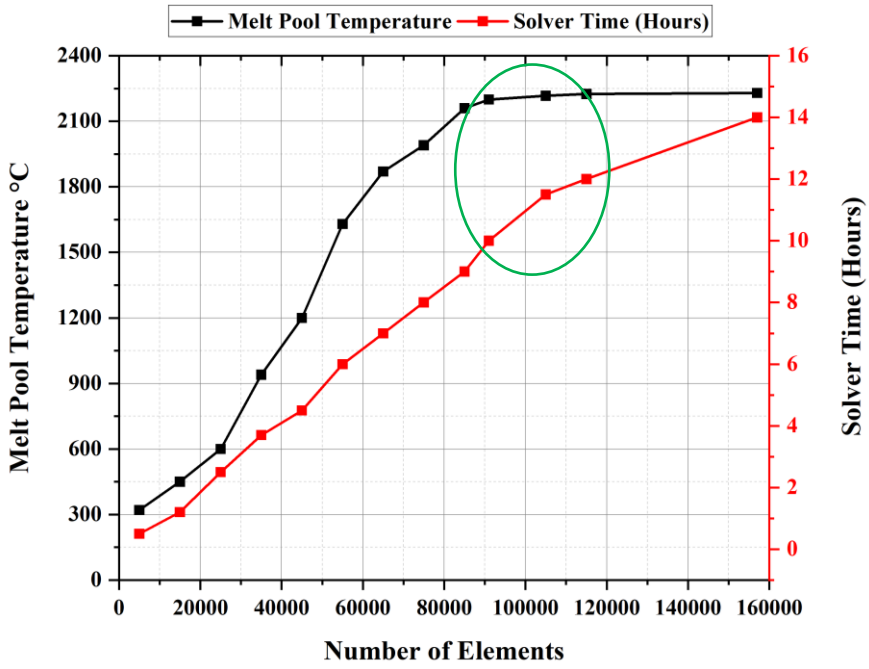

Figure 3.9. Mesh independence illustration

After conducting the analysis, it was found that the optimal mesh configuration for the model was 94,000 grid elements with a time step of 2-5 µs. This configuration ensured that the simulation results were not impacted by the mesh and time step and provided precise and reliable results. The research also estimated the computation time required for the study to be approximately 11 hours. The analysis was executed on an efficient-performance computing workstation, equipped with an Intel Xeon E5530 high performance processor operating at 2.26 GHz and 128 GB of RAM.

This finding highlights the importance of selecting the appropriate mesh configuration and time step in simulations to achieve accurate and reliable results. Inaccurate results can lead to incorrect conclusions, potentially leading to inefficient processes, and may cause issues in the final product. Therefore, it is essential to determine the optimal mesh and time step in any simulation study to ensure accurate results that can be relied on for making informed decisions.

3.6 Properties of SS316L:

The SEM micrograph in Figure 3.10 illustrates the FCC (face-cantered cubic) crystal lattice structure of γ-austenite, which is characteristic of the low carbon stainless steel SS316L. This steel is commonly used in a range of industries, including construction, petrochemicals, pharmaceuticals, nuclear power plants, and orthopaedic implants, due to its superior corrosion resistance, low rate of neutron radiation, and mechanical properties, including strength, fracture toughness, and ductility [82, 83].

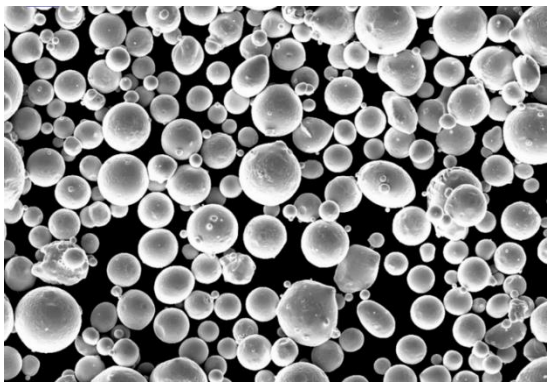

Figure 3.10. Scanning electron microscope image of SS316L

The main components of 316L stainless steel are Cr, Ni, and Mo, which serve as its primary alloying elements. The presence of Cr aids in decreasing susceptibility to uniform corrosion, whereas Ni enhances the alloy's durability and malleability. Additionally, Ni acts as an austenite stabilizer, which keeps the alloy's face-centred cubic structure intact at normal temperatures. The introduction of Mo also reinforces the alloy's ability to withstand localized uniform and pitting corrosion, thus making it more resistant to corrosion in chloride environments [84, 85]. The composition values for the aforementioned alloying elements are displayed n Table 3.1. The high toughness characteristic of 316L SS is attributed to its FCC crystal lattice structure's ductility, which is compared to pure iron's BCC crystal lattice structure. The precipitation of Cr-rich carbides and intermetallic phases, known as sensitization, can impair its corrosion resistance and mechanical properties. However, 316L SS has a low C content (< 0.03 wt. %), which reduces sensitization and is hence labelled "L for Low Carbon". Heat treatments cannot strengthen or harden 316L SS, unlike other stainless steels, because of its low C content. However, cold working can achieve hardening by effectively introducing the work-hardening effect [86].

Table 3.1. Major Alloying elements of SS316L

Element	**Cr**	**Ni**	**Mo**	**Mn**	**Si**	**P**	**C**	**S**	**Fe**
Mass %	16-18	10-14	2-3	2.0	0.7-1	<0.045	0.03	0.03	Balanced

Previous research has indicated that SS316L's thermal conductivity varies non-uniformly in both its powder and solid phases. This non-uniformity is primarily due to the presence of defects, including pores and cracks, that form during the SLM process. The thermal conductivity of SS316L can be expressed mathematically using the following equation [73, 87].

$$k_p = k_s\,(1 - \emptyset) \tag{6}$$

The above equation shows that the thermal conductivity of SS316L is a function of both the solid and powder phases' thermal conductivity and the powder volume fraction. As the powder volume fraction increases, the thermal conductivity of SS316L decreases due to the lower thermal conductivity of the powder phase. Therefore,

incorporating the non-uniformity of SS316L's thermal conductivity into simulation models is crucial for accurate predictions of the SLM process's thermal behaviour. This non-uniformity can significantly impact the temperature distribution, melt pool dimensions, and other critical process variables. Accurate predictions of these parameters are vital for optimizing process parameters and obtaining desired properties in manufactured components.

Similarly, powder and solid phase densities are not similar and rely on the % porosity of the powder particles. The given equation defines the connection between the density of the solid and powder phases [88]

$$\emptyset = \frac{\rho_S - \rho_p}{\rho_S} \quad (7)$$

The temperature distribution was considered in light of the fact that the SLM involves both melting and solidification, which takes into account the influence of latent heat. To address this, enthalpy was employed, and the relationship between enthalpy and temperature is expressed by Equation (8) below [89].

$$H = \int \rho c dT \quad (8)$$

3.6.1 Material Properties of Stainless Steel 316L:

The FEM model for 316L stainless steel utilized temperature-dependent material data presented in Table 3.2. The data encompassed temperature dependent properties i.e. thermal conductivity, specific heat capacity, density, and melting temperature ranging from room temperature to evaporation temperature, including solidus and liquidus temperature. To ensure comprehensive data, certain parameters were interpolated using literature.

To accurately predict the thermal behaviours of a material, incorporating the temperature dependent material properties is critical. The use of accurate data is vital for obtaining reliable simulation results. Temperature-dependent material data is essential because the properties of materials vary with temperature changes. As such, the behaviour of 316L stainless steel at room temperature may be significantly different from that at the liquidus temperature or the evaporation temperature. The

thermal behaviour of the SLM process can be influenced by various factors, including material properties. As a result, incorporating temperature-dependent material data is essential in developing accurate models that can predict the SLM process's behaviour. Therefore, using precise data that accurately captures the temperature-dependent behaviour of 316L stainless steel is crucial for reliable and accurate simulation results.

Table 3.2. Temperature dependent properties of SS316L

Temperature ℃ [90, 91]	**25**	**420**	**850**	**1250**	**1400**	**1450**	**1700**	**2600**
Material Density $\boldsymbol{\rho}$ $(\boldsymbol{kg/m^3})$	7951	7784	7574	7360	7270	7235	6764	6741
Thermal Conductivity $\boldsymbol{k}$ $(\boldsymbol{W/(m.K)}$	13.3	21.9	27.3	30.8	35.9	28.45	30.52	32.22
Specific Heat Capacity C $(\boldsymbol{J/(kg.K)})$	472	561	632	705	734	828	832	955
Enthalpy $\boldsymbol{H}$ $(\boldsymbol{J/g})$	0	191	429	690	823	1128	1254	2590

3.7 Model Calibration:

The SLM process is a complex one, and to obtain reliable results, multiple concurrent processes must be taken into account, as concluded from the discussion. Figure 3.11. illustrates the occurrence of these phenomena.

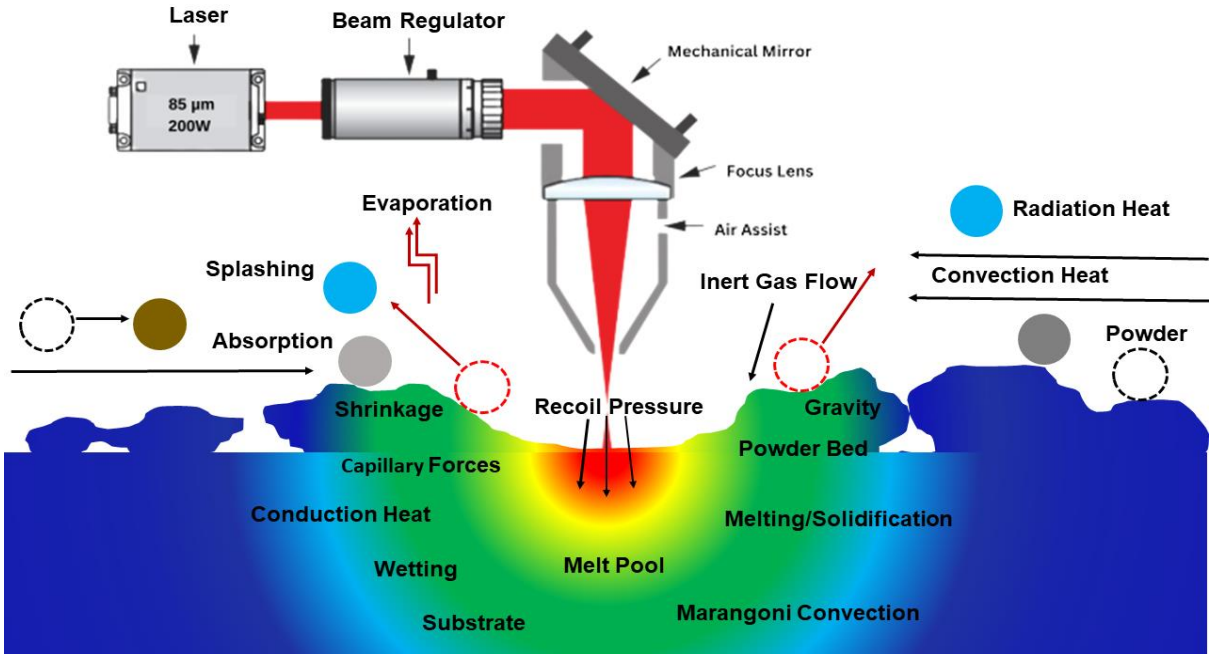

Figure 3.11. Physical phenomenon during Selective laser melting

The current model used for simulating the SLM process incorporates various physical phenomena that affect the melting pool's geometry, such as thermal conduction, heat transfer, and solidification. However, some other phenomena such as wetting, capillary forces, the Marangoni effect, shrinkage, and recoil pressure were simplified or excluded from the model.

Despite their exclusion, these phenomena could still affect the melting pool's geometry, and hence the material thermal conductivity of SS316L was calibrated to incorporate all the ignored or simplified physics and account for its most significant sensitivity. This adjustment was made to improve the accuracy of the simulation results and achieve a closer match with experimental measurements.

The output of the simulation model was compared to experimental measurements, and if a significant difference was observed, the thermal conductivity was further modified to achieve a specific range of deviation between the simulation and measurement. This iterative process of adjustment and comparison was continued until the desired level of accuracy was achieved.

It should be noted that simplifying or excluding certain physics from the simulation model does not necessarily mean that the model is incorrect. Instead, it is a necessary step in simplifying the model to make it computationally feasible. However, adjusting the thermal conductivity to account for these excluded or simplified physics is a critical step in improving the accuracy of the simulation results.

In summary, adjusting the thermal conductivity of SS316L to account for ignored or simplified physics in the simulation model is a necessary step in improving the accuracy of the simulation results. This adjustment is made through an iterative process of comparison with experimental measurements until the desired level of accuracy is achieved.

3.8 FEM Model Validation:

Other studies were referenced to determine the parameters used in the simulations. In order to ensure the accuracy of the FEM model, the other important parameters were implemented according Table 3.3.

Table 3.3. Process parameters for numerical simulations

Process Parameter	**Value**
Power Supplied	180-240W [92-96]
Laser Beam Radius	70-85 µm [92-96]
Laser Scan Speed	950- 1250 mm/sec [92-96]
Hatch Spacing	77.5-85.0 µm [92-96]
Absorptivity	0.36 [97]
Layer Thickness	0.30 µm [98]
Laser Penetration Depth (S)	0.06 mm [33]
SS316L Melting Temperature	1400 °C [49]
SS316L Evaporation Temperature	2800 °C [99]
Convection Heat Coefficient	150 $W/m^2 \times °C$ [100]
Emissivity	0.35

Similarly, Table 3.4. displays the results of the simulated model at various process parameters. These outcomes were compared with the experimental outcomes of

SS316L single and multi-track samples obtained by different researchers. The average dimensions of the melt pool show a reasonable correspondence between the simulation and experimental measurements, validating the precision of the current numerical model.

Table 3.4. Simulated and Experimental melt pool dimensions from literature

S. No	Author	Average Length	Average Width	Average Depth	Maximum Temperature
		µm	µm	µm	K
1	Trejos-Taborda, et al. [101]	-	158.07	98.56	2815
2	Heeling, et al. [97]	-	142.43	97.29	2744
3	Lee and Yun [102]	-	136.27	105.63	3900
4	Ahmed, et al. [95]	368	112.08	66.05	4000
5	Gusarov, et al. [99]	301	200.07	70.02	4800
6	Hodge, et al. [103]	264	208.03	65.21	4900
7	Tran and Lo [98]	225	180.09	68.45	3015
8	**Current Study**	**342**	**139.01**	**92.19**	**2450**

3.9 Experimental Analysis of Melt Pool:

The experimental study utilized the Farsoon FS421M 3D metal printer, which is an advanced AM machine capable of printing high-quality metal parts with exceptional accuracy and precision. The printer features a powerful Ytterbium fibre laser capable of reaching a maximum power of 500W, a 1070 nm wavelength, and a beam diameter ranging from 70-200 µm. By producing a laser beam with a Gaussian energy distribution and a diameter between 70 and 85 µm, the laser source enables the creation of intricate and precise part designs.

The Farsoon FS421M printer is equipped with a build chamber that measures 425mm × 425mm × 420mm, providing ample space for printing large and complex parts. The printer can attain a layer thickness of 0.02-0.1mm with a scanning speed of up to 1500 mm/sec, enabling fast and efficient printing. The system has an accuracy of +/- 50 µm for small parts, and a possible deviation of +/- 0.2% for larger parts, ensuring high dimensional accuracy and repeatability of around 20 µm.

To facilitate the printing process, the Materialise Magics software is available, which streamlines the process of preparing parts, selecting printing strategies, and conducting build simulations. This software aids in optimizing the printing process, and reducing the risk of errors and improving the overall efficiency of the printing process.

To prevent melt pool from oxidation during the printing process, argon gas is utilized as an inert gas to shield the build chamber and the part. This inert gas creates an oxygen-free environment that prevents the metal from oxidizing, resulting in high-quality parts with exceptional mechanical properties.

Figure 3.12. Farsoon 421M PIAM 3D

3.9.1 Optical Microscopy:

The study utilized the Olympus Corporation DSX10 UZH microscope, which is a state-of-the-art imaging device that enables high-resolution visualization of metal parts with exceptional accuracy and precision. The microscope is equipped with a built-in monitor that allows for real-time communication between the user and the

device, enabling the operator to monitor the imaging process in real-time and make any necessary adjustments to optimize the image quality.

One of the key features of the DSX10 UZH microscope is its 360-degree viewing and rotation capability, which allows for flexible focusing from any direction and angle with a depth-of-field of approximately 20 times. This feature enables the operator to easily visualize complex geometries and fine details that may not be visible with other imaging systems.

The microscope can magnify between 0.1x to 5,000x and provides three different resolutions: 1600 x 1200, 3200 x 2400, and 4800 x 3600, at a frame rate of 60 fps and 20 Megapixels. This level of magnification and resolution enables the operator to visualize even the finest details of the metal parts, facilitating the identification of any defects or imperfections that may impact the part's mechanical properties or performance.

Overall, the Olympus Corporation DSX10 UZH microscope is a powerful tool for imaging metal parts, enabling high-resolution visualization with exceptional accuracy and precision. Its 360-degree viewing and rotation capability, high magnification and resolution, and real-time communication with the operator make it an essential tool for quality control and inspection in the additive manufacturing industry.

Figure 3.13. Olympus corporation DSX10 UZH

Chapter 4 Results and Discussions

4.1 Measurement of melt pool:

Figure 4.1, presents a visual representation of the temperature distribution inside a melt pool during the SLM process. As mentioned earlier, the quality of SLM part is predominantly dependent on temperature distribution and dynamic stability of the melt pool, hence, it is considered as a critical factor for characterization. In this figure, we can observe the temperature variation across various regions of the melt pool. The darker red regions correspond to higher temperatures, while the blue regions represent lower temperatures. The temperature distribution within the pool is influenced by various factors such as the laser power, scanning speed, and material properties and is non-uniform posing significant challenges.

The heating and cooling cycles in the melt pool directly affect the size, shape, and lifespan of the pool. The maximum thermal gradient within the pool also affects the solidification process, which commences once the temperature falls below the material's liquidus temperature. The solidification process is important in determining the final grain size, surface quality, and residual stresses in the finished product.

Inadequate melting can result in powder particles remaining unmelted, leading to various porosity defects in the final product. The final manufactured components may contain pores due to minimal melt-pool temperatures. Additionally, a lack of fusion can cause coarse and enlarged pores, which also affects the quality of the finished product. Therefore, it is crucial to have a uniform temperature distribution within the melt pool to ensure a high-quality final product [43].

Conversely, high temperatures can cause excessive heat stresses, overcooking, splatter, and keyholes. At elevated thermal applications, material evaporation may occur resulting in loss of key elements and potential keyholes. The other parameters i.e., surface roughness, porosity, and mechanical properties of components manufactured by SLM are dependent on the percentage of overlap between tracks and

layers is a critical factor that significantly affects the final part properties as well. Therefore, it is important to thoroughly evaluate melt-pool characteristics, temperature gradients, and intertrack and interlayer overlap to minimize the occurrence of such defects. Overall, the temperature distribution within the melt pool is a crucial factor that significantly impacts the final quality of the manufactured parts.

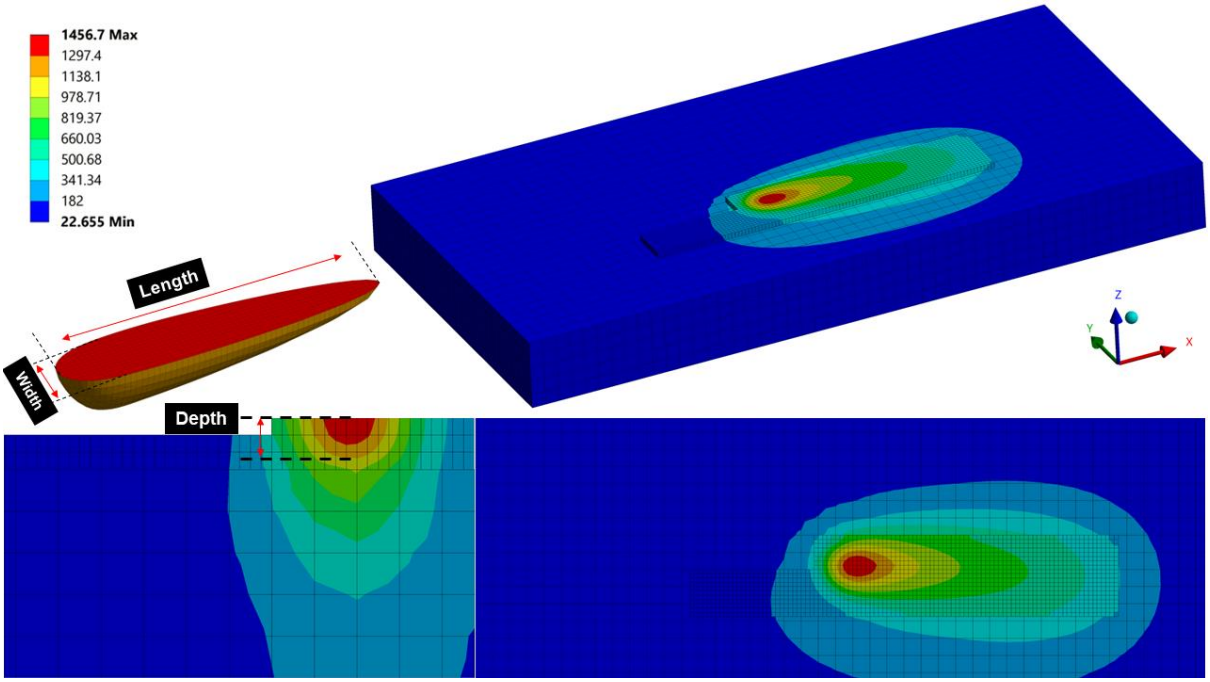

Figure 4.1. Simulated Melt pool overview

4.2 Inter Layer Effect:

During the real SLM process, each layer is melted and solidified sequentially with each subsequent layer being added on top of the previous one. This results in the formation of a layered microstructure with a distinct interlayer region, which can significantly affect the overall properties of the final part.

The interlayer region is the region between two adjacent layers where the heat-affected zone (HAZ) from the previously deposited layer interacts with the current layer being melted. During the SLM process, due to the energy input from the laser the temperature of the metal powder in the previous layer rises to a high level. This temperature rise can lead to melting, and in some cases, even vaporization of the metal

powder in the HAZ. The resulting molten material can then diffuse into the current layer being melted, leading to changes in the microstructure and properties of the part.

One of the most significant effects of the interlayer region is the formation of interlayer porosity. The interlayer porosity is caused by the entrapment of gases, such as oxygen and nitrogen, that are released during the SLM process. When trapped in the molten metal, these gases may create voids or pores upon solidification. The existence of such interlayer porosity can considerably diminish the part's strength and ductility, rendering it more susceptible to failure.

During the SLM process, the metal in the previous layer cools down and solidifies, forming a columnar grain structure, which is yet another interlayer defect. This columnar structure can propagate into the current layer, leading to an elongated grain structure that is oriented perpendicular to the build direction. This orientation can significantly affect the overall properties of the part, particularly in terms of anisotropy, where the properties of the part vary depending on the direction of loading.

To mitigate the effects of the interlayer region, several strategies can be employed. One common approach is to use multiple lasers passes to remelt and homogenize the interlayer region, reducing the amount of interlayer porosity and columnar grains. Another approach is to vary the process variables, to control the heat input and reduce the HAZ size. Finally, post-processing techniques such as hot isostatic pressing (HIP) or annealing can be used to improve the density and mechanical properties of the part, particularly in the interlayer region.

Figure 4.2. illustrates the temperature variation at various points in the SLM process for specific parameters. The temperature measurements were taken at different depths in the Z direction, from 0.030 mm to 0.450 mm, at fixed coordinates (X=0.50, Y=0.250) on 15 layers labelled L1 to L15, with a thickness of 30.0 µm each. The other parameters used in the experiment include a scan speed of 1080mm/sec, a hatch spacing of 77.50 µm, laser power of 220W, and a laser beam radius of 80 µm.

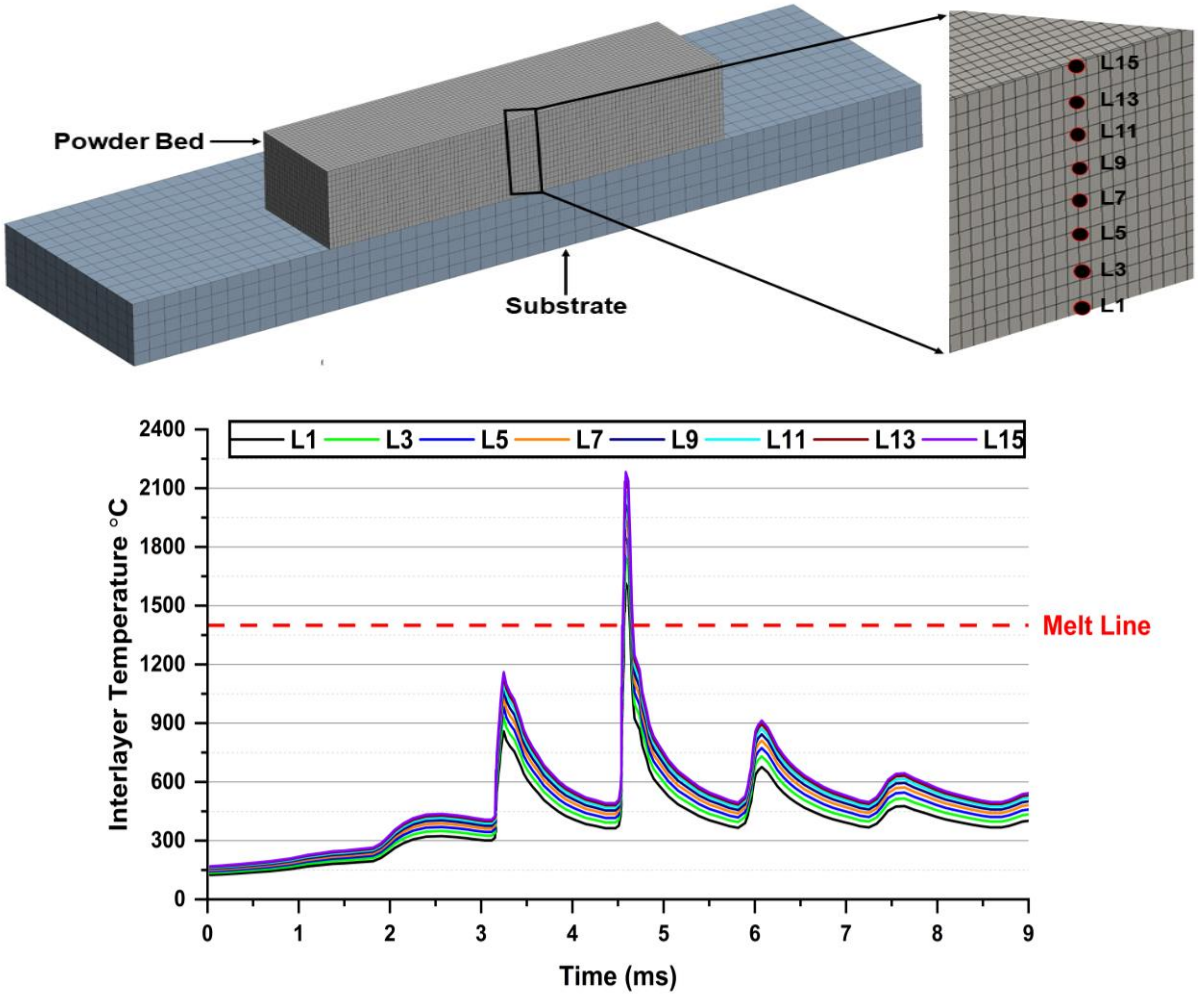

Figure 4.2. a). A sectional view of the simulated model, featuring points for evaluating inter-track effects. b) Inter-track temperature readings (°C).

As shown in the graph, the melt pool maximum temperature increases with the progression of layers from L1 to L15. This is due to heat accumulation and pool expansion. The temperature rises between the first ten layers remained consistent, ranging from 15-45 °C, but the thermal rise is limited to only 3-5 °C for subsequent layers. The findings align with earlier experimental and numerical studies that employed various laser configurations.

The graph provides insights into the thermal history and interlayer effects at specific positions in the layers for the given parameters. The results obtained from this experiment can be utilised to optimize the process variables to achieve a uniform thermal gradient within the melt pool and minimize defects in the final printed product.

The melt pool shape geometry and shape play a significant role in determining the quality of the final product. The melt pool dimensions increase with number layers of layers and is not consistent within a layer. To analyse the variation in the size of the melt pool across the layers, Figure 4.3. and Figure 4.4. present the dimensions of the melt pool for each layer, ranging from L1 to L15.

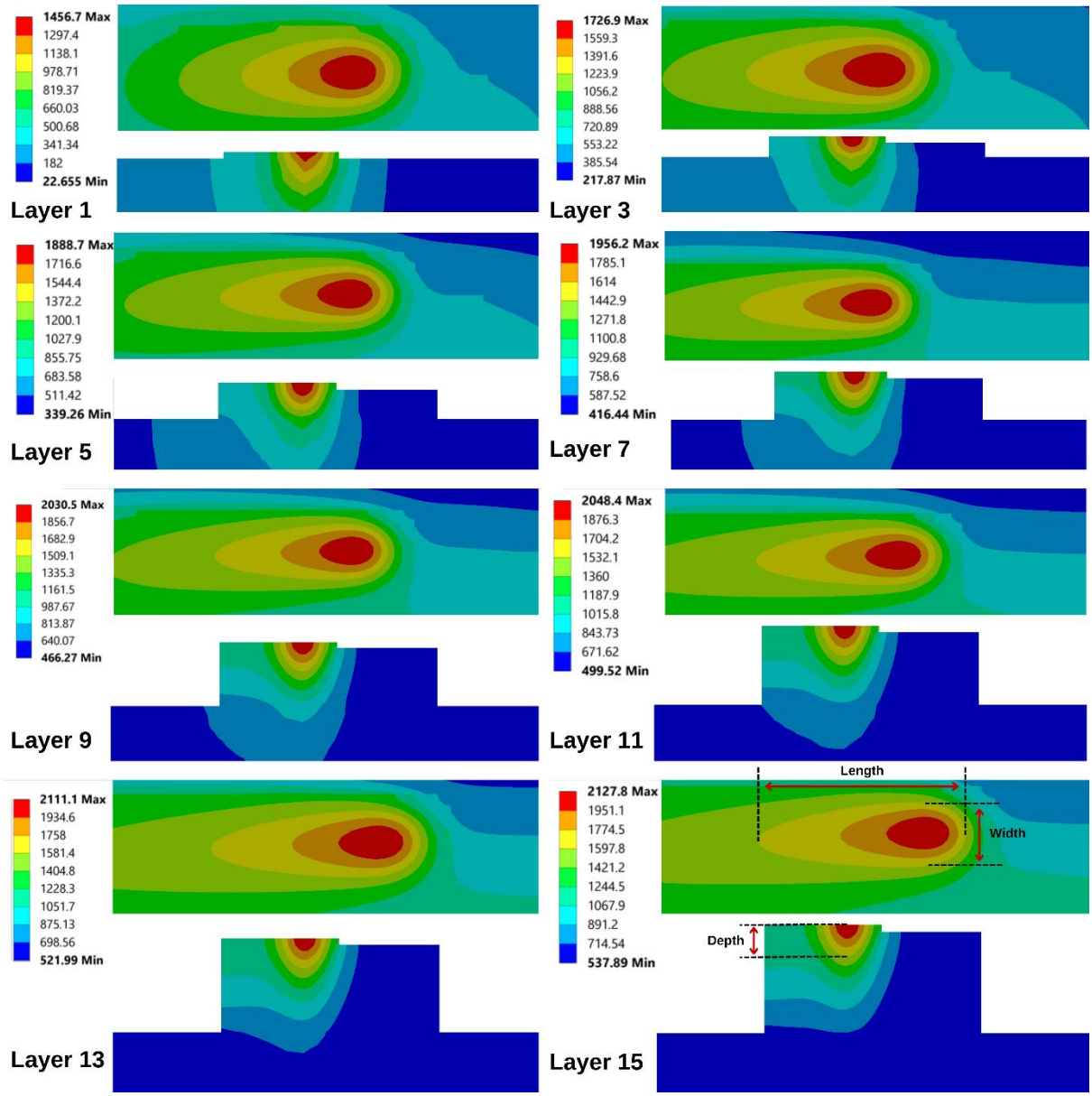

Figure 4.3. Simulated inter-layer melt pool variation

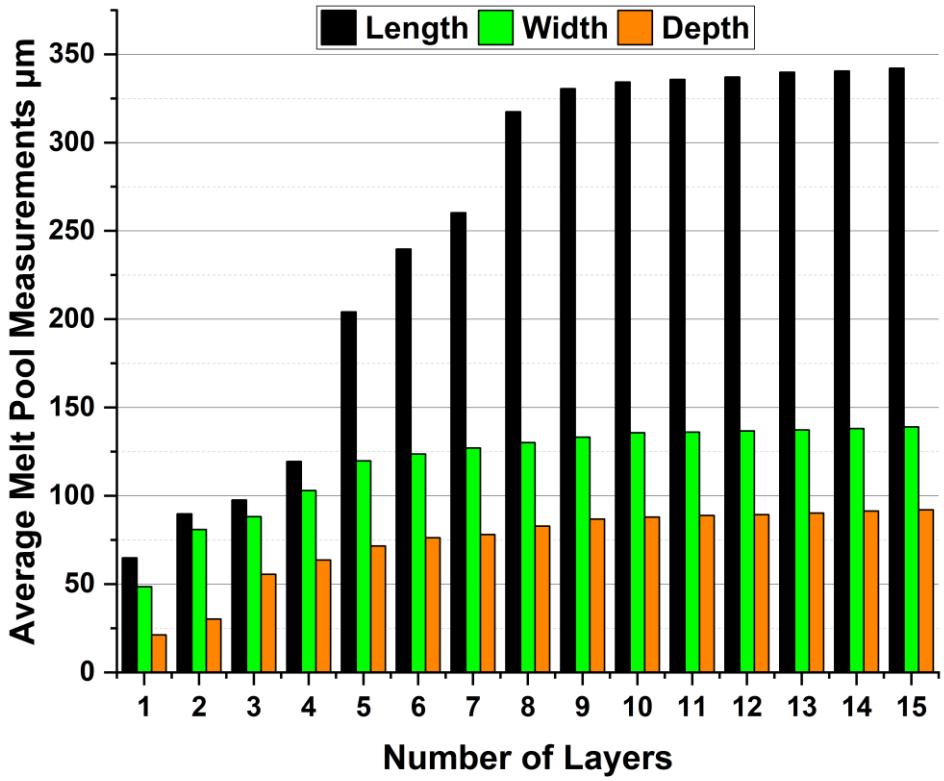

Figure 4.4. Simulated Inter-layer Melt Pool Measurements

The figures indicate that the melt pool size increases considerably as the number of layers increases. The molten pool length increases from 85.84 µm in the first layer to 347.45 µm in the 15th layer. Similarly, the width increases from 56.30 µm in the first layer to 142.55 µm in the 15th layer. The depth of the pool also increases substantially from 17.21 µm in the first layer to 92.15 µm in the 15th layer. The outcomes are in line with earlier investigations that have documented a rise in the size of the melt pool with an increase in the number of layers.

However, it is important to note that the median variation in the dimensions of the melt pool becomes insignificant after the 10th layer. The variation is only 0.5-1.5 µm, which suggests that the SLM process has reached a steady-state after the 10^{th} layer deposition. This implies that the size of the melt pool remains relatively constant beyond a certain layer number, which is an important consideration for process control and optimization.

4.3 Inter Track Effect:

In selective laser melting (SLM), inter-track effects refer to the influence that previously deposited metal tracks have on subsequent tracks during the SLM process. Inter-track effects significantly impact the quality and integrity of the final SLM part, and therefore, understanding and controlling them is critical for producing high-quality parts.

One of the primary inter-track effects in SLM is the heat accumulation effect. When the laser moves across the powder bed, it heats and melts the same section of the material repeatedly. This leads to heat accumulation, which can cause thermal stresses and distortion in the part. Excessive heat accumulation can lead to several defects in the final part, including cracking, porosity, and other imperfections.

Another inter-track effect is the balling effect, which occurs when molten metal from one track flows into the previously deposited track, forming a small ball of material. Balling can result in reduction in the density of the final part, as well as defects such as voids and inclusions.

The overlap effect is another inter-track effect, which occurs when adjacent tracks overlap during the SLM process. Overlapping can lead to the development of solidification defects, such as voids and inclusions. Overlapping can also cause a reduction in the surface finish of the final part.

To mitigate inter-track effects, various strategies can be used during the SLM process. For example, adjusting the scanning patterns, the laser power, scan speed, and beam diameter, can help control the heat accumulation effect. Similarly, optimizing the powder bed preparation and controlling the powder layer thickness can help reduce the balling effect. Overlapping can be minimized by optimizing the scanning strategy, such as adjusting the overlap distance between adjacent tracks.

In summary, inter-track effects critically impacts the SLM process, and understanding and controlling them is essential for producing high-quality parts. By optimizing the scanning parameters, powder bed preparation, and scanning strategy, inter-track

effects can be minimized, resulting in components with improved properties and dimensional accuracy.

Figure 4.5. presents the temperature distribution in successive tracks and the intertrack effect on temperature for the given process parameters. The temperature measurements were taken at six points, labelled as T1 to T6, while maintaining the Y and Z positions constant and varying the X position. The hatch separation between the tracks was 77.50 µm. The results showed that the temperature at each point gradually increased and then decreased as the laser scanned over it. This behaviour is due to the laser's thermal energy absorption and dissipation into the surrounding material. The intertrack effect was also evident, with the temperature at T1 being influenced by the previous track's heat input. The temperature at T1 was observed to be lower than at T2, indicating that the heat from the previous track had already dissipated. Similarly, the temperature at T6 was higher than at T5, showing that the heat from the previous track was still present.

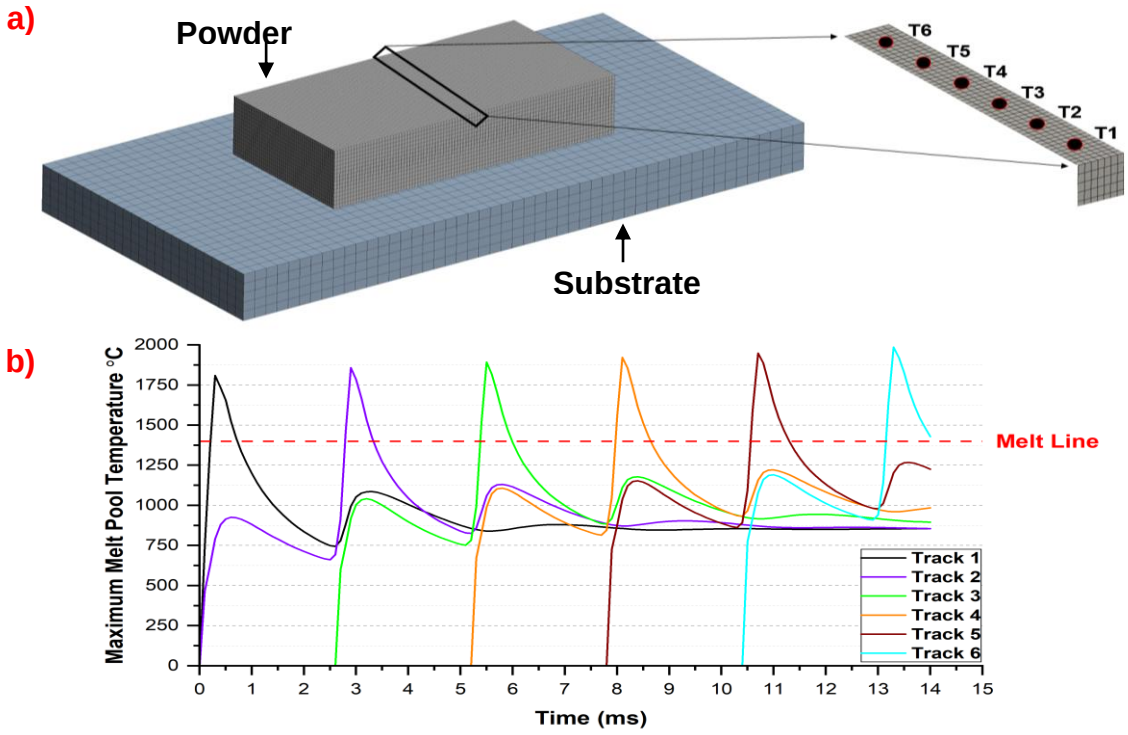

Figure 4.5. A sectional view of the simulated model, featuring points for evaluating inter-layer effects. b) Inter-layer temperature readings (°C).

The intertrack effect can be seen in the melt pool temperature distribution. The temperature at T1 is the minimum, and it gradually rises with each subsequent track until it reaches its highest point at T6. The peak temperature at T6 is significantly higher than the initial temperature at T1. This temperature increase is due to the heat accumulation effect, where the heat input from multiple scans is added to the already heated region. This heat accumulation effect is more pronounced in regions where neighbouring tracks melt the same area twice. The overlapping of adjacent tracks results in the hatch spacing, which is responsible for creating a fully dense layer.

The temperature rise between successive tracks is consistent, ranging from 30-40 °C. This rise is due to the cumulative heat input from each scan, which increases the temperature of the melt pool. The temperature increase in the melt pool is more pronounced in the areas where multiple scans overlap, resulting in a higher temperature rise.

With the addition of more tracks, the temperature of the previously deposited tracks drops below the melting point of the SS316L material. This is due to the cooling effect caused by the lack of direct heat input from the laser as it traverses over the previously melted areas. This temperature difference between the newly deposited tracks and the previously deposited tracks could potentially affect the final material properties of the component being built.

The analysis of the intertrack effect and temperature distribution in successive tracks provides important insights into the SLM process. These insights can be used to optimize the process variables, such as scan speed, laser power, and hatch spacing, to improve the final part's quality.

Figure 4.6 and Figure 4.7. provide an analysis of the dimensions of the melt pool as the laser moves along the tracks within the same layer. The melt pool characteristics are critical in determining the quality and properties of the final part produced by the SLM process. The width and length of the melt pool are critically determining the surface finish of the final part, while the depth of the melt pool is essential in controlling the melting and solidification behaviour of the metal powder.

The data provided in the figures show that the melt pool width increase as the laser moves along the tracks within the same layer. The width of the increases by 11.50 µm between the 1st and 2nd tracks, followed by an increase of 7.29 µm between the second and third tracks. The third to sixth tracks show a consistent increase of 0.55-1.50 µm in the width of the molten pool. The length of the melt pool varies greatly, with an increase of 115 µm from T1 to T6. The intertrack increment in the length of the melt pool is 25-40 µm up to the 3rd track, but the variation is limited to only 0.5-5 µm in the subsequent tracks. Unlike the width and length, the depth of the melt pool doesn't increase substantially as the laser traverses along the tracks within the same layer. This trend indicates that the laser energy input is sufficient to maintain a constant melt pool depth. The uniformity of the melt pool depth is determining the part quality and reproducibility of the SLM process.

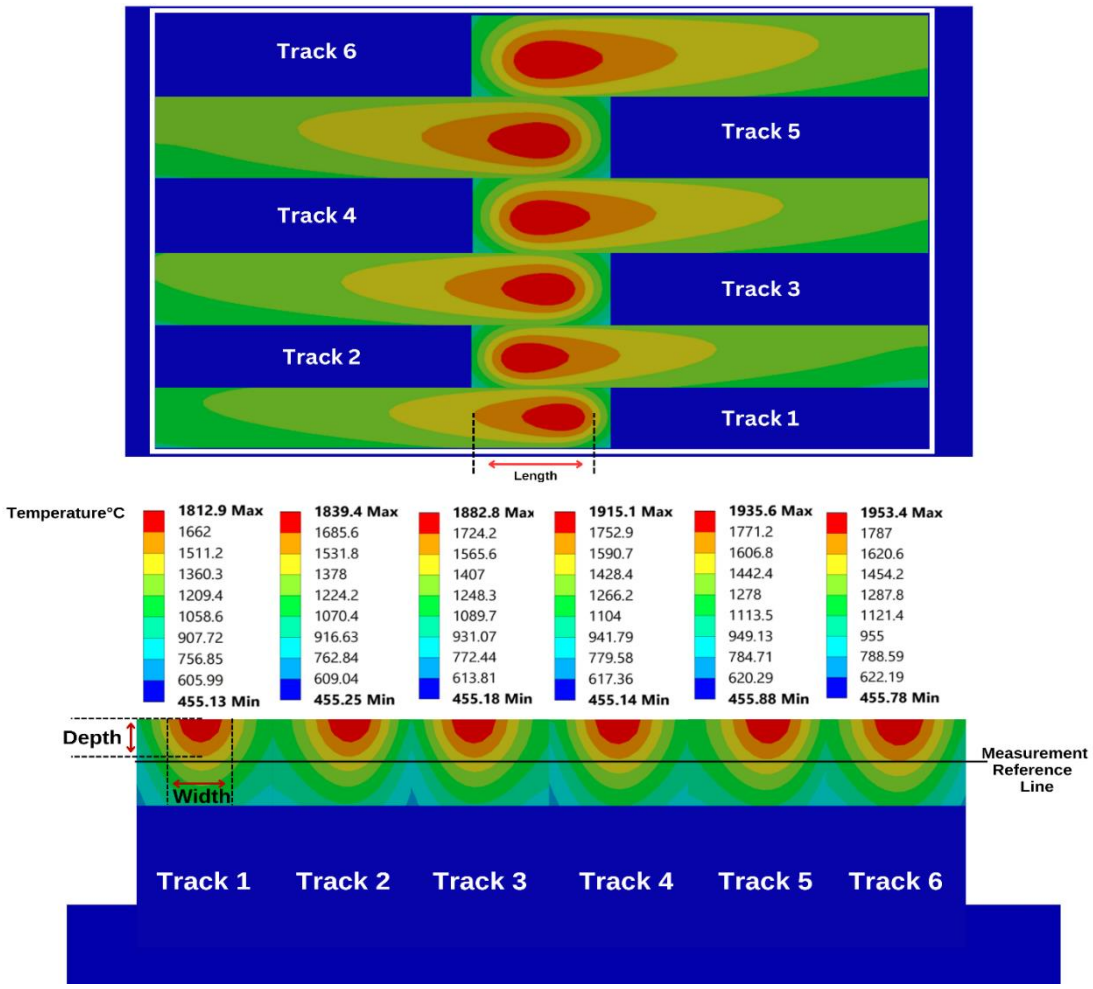

Figure 4.6. Simulated Inter-layer Melt Pool Variation

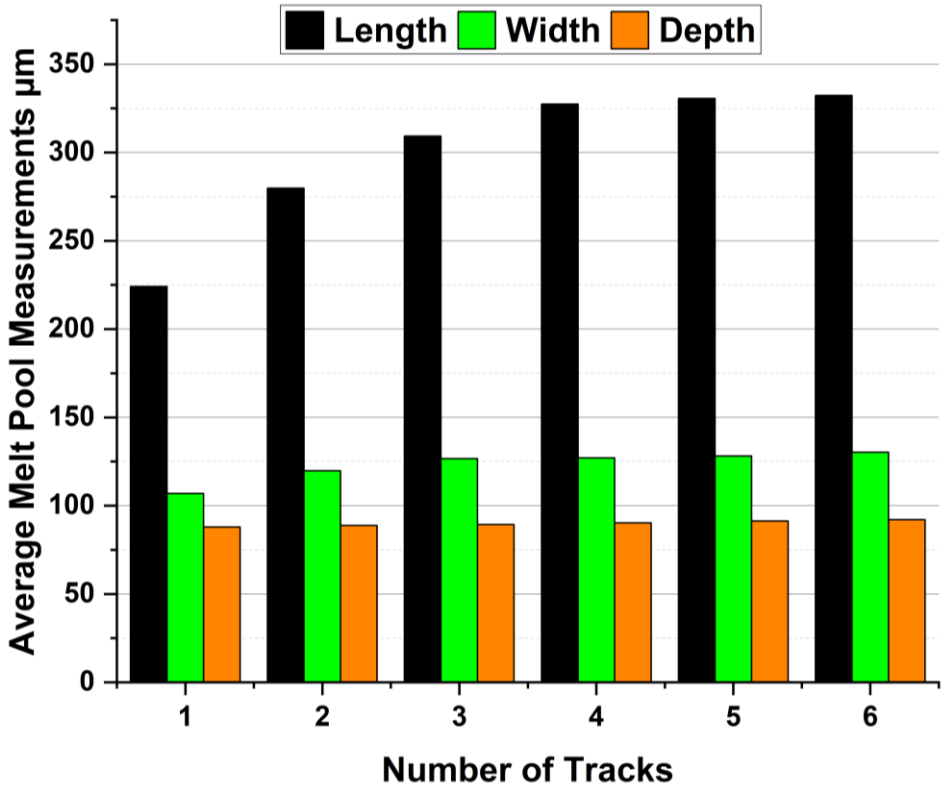

Figure 4.7. Simulated Inter-Track Melt Pool Dimensions

This analysis provides useful information for optimizing the process variables, such as adjusting the laser power or scan speed, to achieve a more consistent temperature distribution within the melt pool and reduce the intertrack effect. A more uniform temperature distribution can lead to a higher quality printed product with fewer defects. The intertrack effect is an important factor in determining the surface roughness and the mechanical properties of the printed part. Therefore, minimizing its impact is essential in achieving a high-quality printed part. The findings from this study can be useful for designing more effective strategies to optimize the SLM and improve final part quality.

4.4 Effect of process parameters:

Table 4.1. shows the proposed process variables for SLM processing SS316L are the result of a thorough investigation through numerical and experimental evaluations. Several FEM simulations were conducted to examine the impact of various process variables, and the results were compared to experimental data. The researchers were able to identify a favourable set of ideal parameters and factor levels for SLM processing SS316L.

Table 4.1. Process parameters for simulations

Parameter	Range	Step Size	Levels
Scanning speed	950-1250 mm/s	100 mm/s	4
Laser power	180-240 W	20 W	4
Laser beam radius	70-85 µm	5 µm	4
Hatch spacing	77.5-85 µm	2.5 µm	4
Layer thickness	30 µm (Constant)	-	-

These parameters were found to produce parts with good mechanical properties, such as high density, low porosity, and good surface finish.

Note that the ideal parameters may vary depending on the specific material and application. However, this study provides a useful starting point for optimizing the SLM process parameters for SS316L. The suggested parameters can be utilised as a benchmark for future studies and practical applications.

Temperature control during the SLM process is critical in achieving a high-quality final product, as it impacts the microstructure, finished part properties, and porosity of the manufactured parts. Thermal filed inside the melt pool is influenced by various process variables, including the laser power, scan speed, hatch spacing, and laser beam radius. Therefore, optimizing these parameters can significantly impact the quality of the finished product.

The laser power is the primary driver of the temperature field, with an increase in power leading to a gradual temperature rise in the melt pool. However, a higher power

setting can also result in the melting of the previously deposited tracks, resulting in increase in porosity and surface roughness. By regulating the amount of heat input into the material, the temperature is impacted by the scanning speed. A higher scan speed reduces the amount of time the material is exposed to heat, resulting in a lower temperature in the melt pool. However, a higher scan speed also reduces the energy input, leading to a reduction in the melt pool's depth.

The inter-track hatch spacing and laser beam radius also significantly impacts the temperature distribution in the melt pool. A smaller hatch spacing leads to a higher melt pool temperature, because the previously deposited tracks take less time to cool down. Similarly, a smaller laser beam radius increases the temperature by concentrating the energy input into a smaller area.

The maximum melt pool temperature is inversely proportional to these parameters. Therefore, adjusting these parameters can lead to the desired melt pool properties and thermal gradient. Moreover, the temperature field and melt pool follow the laser's path, with a higher thermal gradient in front of the heat source center than behind it. This results in the formation of a thermal gradient between the solid and liquid phases, which can impact the final product's grain structure and mechanical properties.

In conclusion, optimizing the process parameters to achieve the desired temperature field is critical in achieving a high-quality final product in SLM. Among other factors, the temperature distribution can be modified by manipulating the laser power, scan speed, inter-track hatch spacing, and laser beam radius.

4.4.1 Laser Scan Speed:

The scan speed refers to the speed at which the laser beam moves across the powder bed to melt the metal.

The scan speed in SLM is an important parameter because it affects various aspects of the manufacturing process, such as the quality overall properties of the final part, as well as the productivity and efficiency of the process.

When the scan speed is too low, the laser dwell time on each spot is longer, which can lead to excessive heat generation in the powder, resulting in a larger heat-affected zone (HAZ) and increased residual stresses. This may negatively impact the parts properties, causing distortion, cracking, or porosity. Moreover, low scan speeds can significantly increase the build time, reducing the productivity of the SLM process as well.

Conversely, insufficient fusion or incomplete melting between the layers may occur if the scan speed is excessively high, causing inadequate melting of the powder. This can result in weak interlayer bonding and reduced part quality. Additionally, high scan speeds can also lead to increased thermal gradients, which can result in distortions and induced thermal stresses.

Therefore, finding an optimal scan speed is crucial to achieve a balance between quality, productivity, and efficiency in the SLM process. Several factors, such as the material properties, layer thickness, laser power, and other process parameters, influence the ideal scan speed. Researchers and manufacturers continuously explore the effects of scan speed on part quality and productivity to optimize the SLM process and produce parts with desirable properties.

Figure 4.8, illustrates that the dimensions of the melt pool during SLM processing are significantly influenced by the scanning speed. Increasing the scanning speed causes a decrease in the width and depth of the melt pool, while increasing its length. The reason behind this phenomenon is that a faster scanning speed leads to a shorter laser exposure time on the powder bed, which results in insufficient melting and coalescing time for the powder, culminating in a shallower and narrower melt pool.

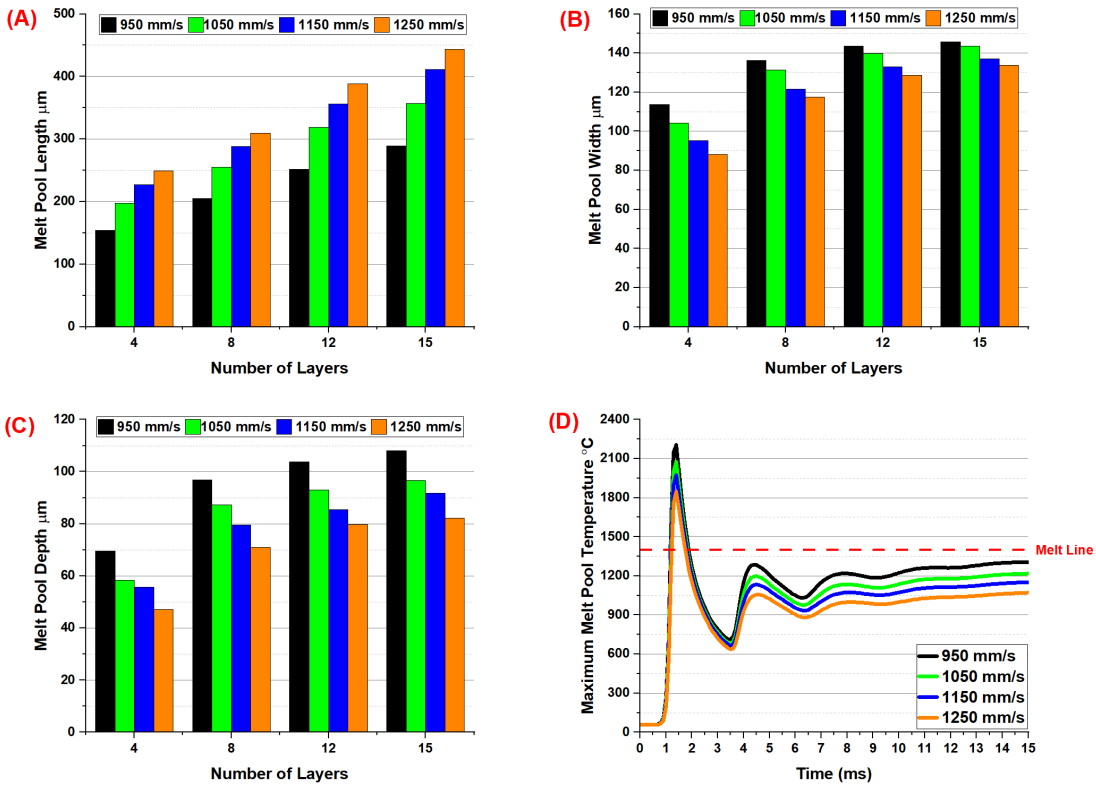

Figure 4.8. Effect of scan speed on melt pool dimensions. (A). Length, (B). Width, (C). Depth, (D). Melt pool temperature profile °C

Measured on the 15th layer, the melt pool length increased from 281 µm at a scanning speed of 950 mm/sec to 443.0 µm at a scanning speed of 1250 mm/sec. This demonstrates that increasing the scanning speed can result in longer melt pools, which could affect the final properties of the part.

Furthermore, as the scanning speed increases, the width and depth of the melt pool decrease. For example, in the 15th layer, the width of the melt pool decreased from 146.01 µm at a scanning speed of 950 mm/sec to 135.03 µm at a scanning speed of 1250 mm/sec, while the melt pool depth decreased from 108.05 µm to 82.06 µm. This is because a higher scanning speed leads to less energy being deposited into the powder bed, resulting in less powder melting and coalescing to form the melt pool.

4.4.2 Laser Power:

In SLM, laser power is an important parameter that greatly influences the quality and properties of the printed parts. It denotes the quantity of energy dispensed by the laser per unit time, typically measured in watts (W).

The laser power greatly affects the melt pool depth and width, which in turn affects the surface finish, porosity, and density of the printed part. Higher laser power leads to wider and deeper melt pools, which can lead to better part consolidation and reduced porosity. However, excessive laser power can also cause overheating, evaporation of material, and thermal stresses, which can lead to cracking, warping, and other defects.

The optimal laser power depends on several factors such as the material being printed, the powder layer thickness, the scanning speed, and the spot diameter of the laser beam. Generally, a lower laser power is preferred for thin layers and high scanning speeds to ensure proper melting and solidification without overheating. On the other hand, thicker layers may require higher laser power to achieve proper melting and fusion.

In Figure 4.9, the melt pool characteristics for laser powers ranging from 180W-240W are displayed. The melt pool dimensions were estimated through simulations and then compared with the parameters determined experimentally. The results showed a linear increase in all parameters with an increase in laser power.

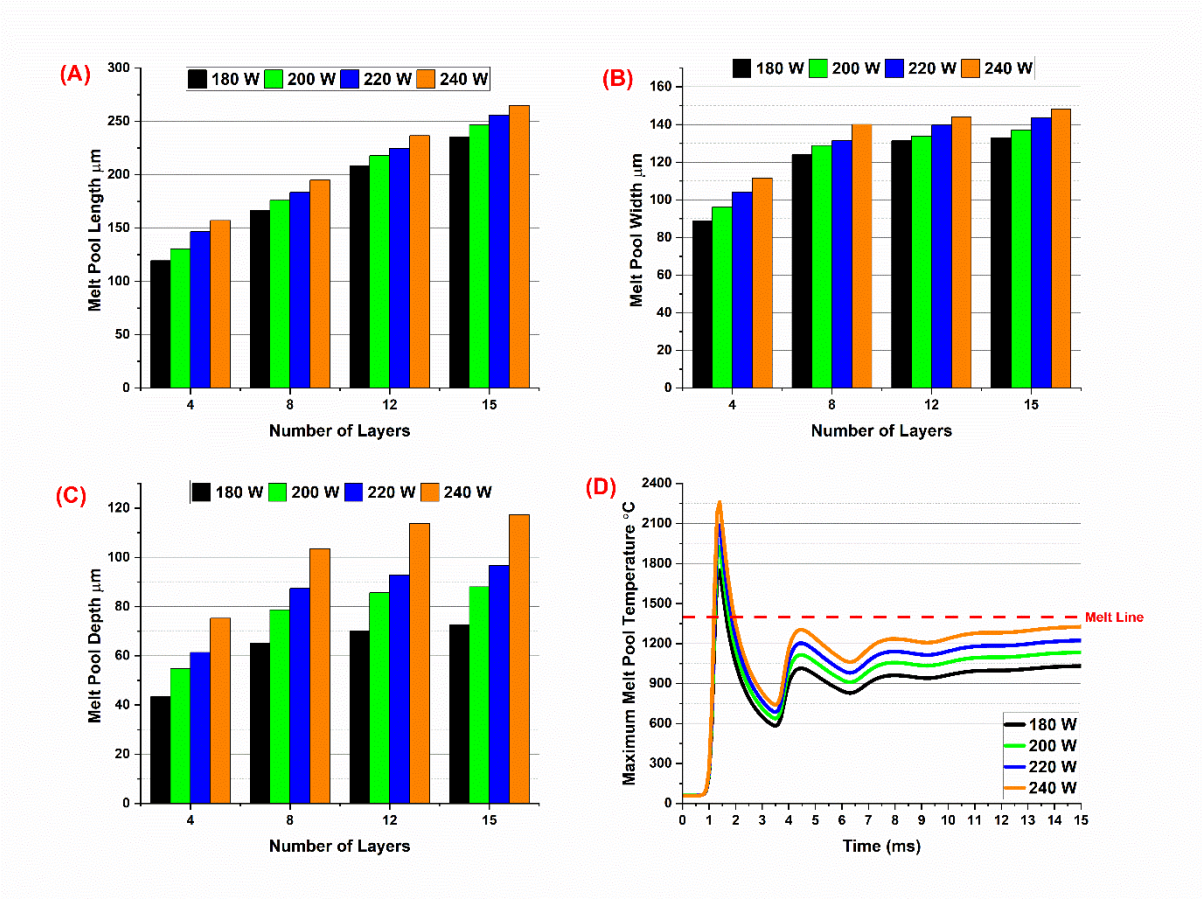

Figure 4.9. Effect of laser power on melt pool dimensions. (A). Length, (B). Width, (C). Depth, (D). Melt pool temperature profile °C

Specifically, the melt pool width increased from 134.05 µm to 147.01 µm, and the depth rose from 73.03 µm to 117.09 µm as the laser power increased from 180W to 240W. Similarly, the length of the melt pool increased from 291.01 µm to 378.05 µm for 180W and 240W, respectively. However, the increase in length was not as significant as the changes in width and depth. The experimental outcomes corresponded well with the simulation data, affirming the precision of the simulation model.

4.4.3 Laser Beam Radius:

The laser beam radius refers to the diameter of the laser beam as it is focused onto the surface of the powder bed. In (SLM), the laser beam radius plays a critical role in determining the accuracy and quality of the final parts produced.

A smaller laser beam radius can produce finer details and higher resolution parts, as it allows for more precise control over the delivered amount of energy to each point on the powder bed. However, a smaller beam radius also means that the laser has to travel more slowly across the powder bed, which can increase the overall processing time and reduce the productivity of the SLM machine.

On the other hand, a larger laser beam radius can allow for faster processing speeds and higher productivity, but at the expense of part resolution and detail. This is because a larger beam radius delivers more energy to each point on the powder bed, which can cause the powder to melt and fuse together more quickly, potentially leading to lower resolution and accuracy.

Therefore, finding the right balance between laser beam radius and processing speed is crucial in SLM to ensure that the final parts have the desired accuracy and quality while also maintaining high productivity and efficiency. This requires careful optimization and calibration of the SLM machine process variables, such as laser power, scan speed, and hatch spacing, to achieve the optimal beam radius for a given application.

As the laser travels forward, the region beneath it liquefies, while the surrounding area cools and solidifies when the laser is directed onto a surface. The solidification process initiates when the thermal gradient decreases below the melting point and continues until it reaches the room temperature. The temperature gradient is the highest at the beginning of the solidification process, whereas it is the lowest towards the end. The rapid solidification of the substrate tracks provides greater stability to the areas of molten and heat-affected zones near the laser point. The multiple reflection phenomenon causes powder particles to exhibit superior optical penetration depths compared to bulk materials. The numerical analysis results demonstrate that the laser

beam radius and the maximum temperature gradient have an inverse relationship; a wider beam radius results in lower temperatures, and a narrower beam radius leads to higher temperatures. In contrast, the increase in laser beam radius leads to a reduction in the melt pool depth, while the length and width demonstrate a linear progression.

Figure 4.10, demonstrates the effect of laser beam radius on the molten pool characteristics. The melt pool length, width, and depth of the melt pool were estimated for two different laser beam radii of 0.70 µm and 0.85 µm. The findings demonstrated that the projected length of the melt pool expanded from 268 µm to 385 µm as the beam radius increased from 0.70 µm to 0.85 µm. This is expected since a larger beam radius would cover a larger area and lead to a longer melt pool.

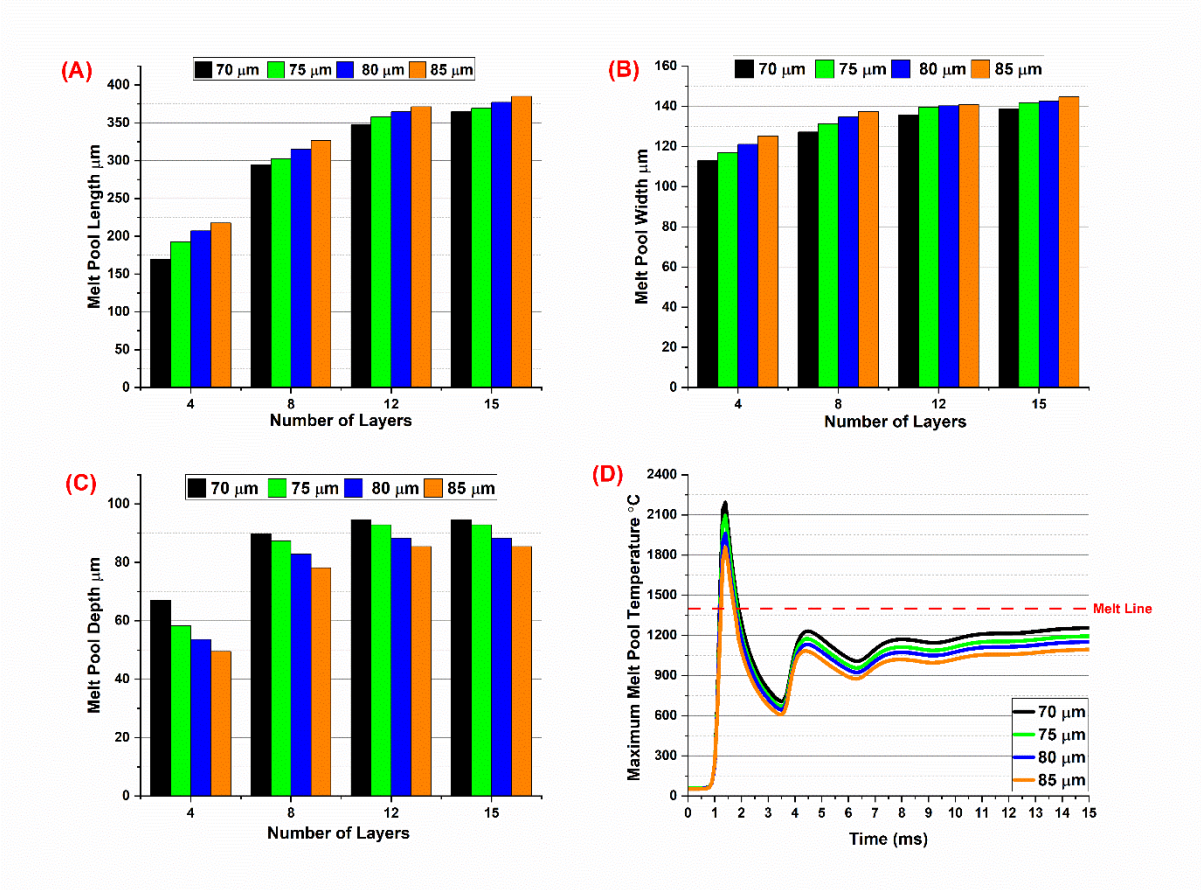

Figure 4.10. Effect of spot radius on melt pool dimensions. (A). Length, (B). Width, (C). Depth, (D). Melt pool temperature profile °C

On the other hand, the melt pool width showed a slight increase from 142 µm to 146 µm as the beam radius increased from 0.70 µm to 0.85 µm. This may be due to the fact that a larger beam radius would lead to a wider melt pool.

However, the projected depth of the melt pool exhibited an inverse correlation with the beam radius. It decreased from 97 µm to 92 µm as the beam radius increased from 0.70 µm to 0.85 µm. This is likely due to the fact that a larger beam radius would result in a shallower melt pool.

4.4.4 Hatch Spacing:

Hatch spacing is an important process parameter in (SLM) that affects the quality and properties of the fabricated parts. It refers to the distance between two consecutive laser scan tracks, and it is typically measured by the center-to-center distance between these tracks.

In SLM, the hatch spacing determines the amount of overlapping between the laser scans, which affects the grain structure, surface roughness, and mechanical properties of the fabricated parts. A smaller hatch spacing results in more overlapping between the laser scans, which leads to a higher density of the parts, a smoother surface finish, and better mechanical properties. However, using a smaller hatch spacing also increases the processing time and the likelihood of defects such as balling and keyholing. On the other hand, a larger hatch spacing reduces the processing time and the risk of defects, but it also results in a lower density of the parts, a rougher surface finish, and inferior mechanical properties. Several factors, including the material, laser power, scan speed, and layer thickness, influence the ideal hatch spacing. It is typically determined through experimental testing and optimization to achieve the desired balance between processing time and part quality.

The temperature profile suggests an inverse relationship between hatch spacing and temperature, as when the temperature decreases the hatch spacing increases. At a hatch spacing of 77.5 µm, the maximum temperature recorded was around 2095°C. As the hatch spacing increases to 80.0 µm, 82.50 µm, and 85.0 µm, the melt pool temperature gradually decreases to 2084°C, 2077°C, and 2074°C, respectively. The amount of

overlap between neighbouring scanning paths is determined by the hatch spacing, and increasing it may result in certain areas along the scanning path being scanned twice. This results in the previously solidified track from the first scan to remelt and solidify again, producing a dense, layered structure. Variations in the hatch spacing can affect the size of the melt pool, but due to the negligible thermal alteration within the pool, the overall difference in dimensions is only between 1 to 5 µm. The powder bed temperature plays a significant role in the metallurgical bond between neighbouring scanning tracks, and an increase in temperature leads to adequate melting of powder particles, producing a strong bond.

The impact of varying hatch spacing on the melt pool dimensions was investigated, and the results are depicted in Figure 4.11. The dimensions of melt pool i.e., length, width, and depth, were estimated using simulations for hatch spacings ranging from 77.5 µm to 85 µm. Surprisingly, the results showed that the range of hatch spacing did not produce a notable variation in the overall dimensions of the melt pool.

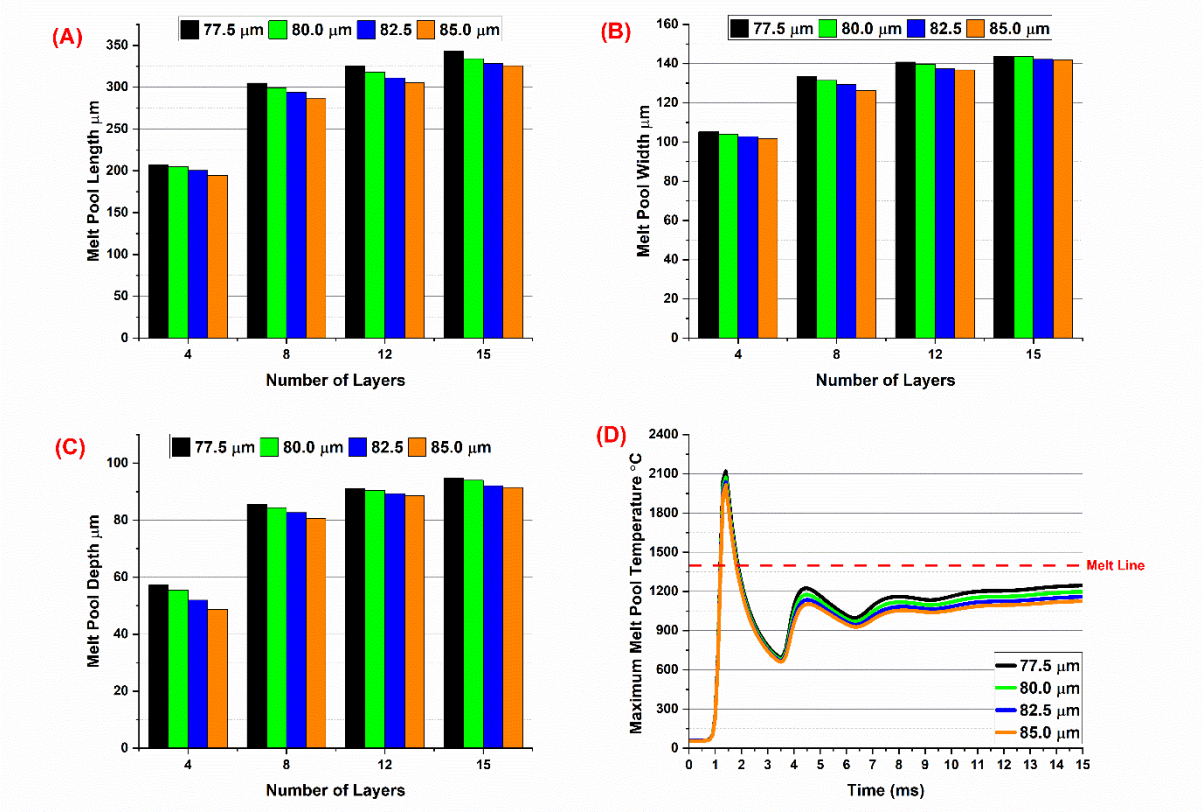

Figure 4.11. Effect of hatch spacing on melt pool dimensions. (A). Length, (B). Width, (C). Depth, (D). Melt pool temperature profile °C

The length of the melt pool reduces from 349.05 to 320.03 µm, as the hatch spacing increases from 77.50 µm to 85.0 µm. This decrease is not significant and can be considered negligible. Also, the predicted width decreases from 143.63 µm to 141.42 µm, which is also a minor change. Similarly, the depth diminishes from 94.76 µm to 90.42 µm within the same hatch spacing range. This reduction is more pronounced than the changes in length and width, but it is still relatively small.

4.5 Melt pool dimensions (Experimental):

To validate the numerical model experimentally, and to predict the size of the melt pool, the experimental setup is depicted in Figure 4.12. The experiments were conducted using a Farsoon FS421M 3D metal printer equipped with a fibre laser. The laser used in the experiments had a power range of 100-500W, a scan velocity of 500-1500 mm/sec, a laser beam diameter between 70-200 µm, and a layer thickness ranging from 25-200 µm. The substrate temperature during the experiments was maintained at approximately 22°C. To avert the oxidation of the powder material, the experiments were performed in an environment based on nitrogen.

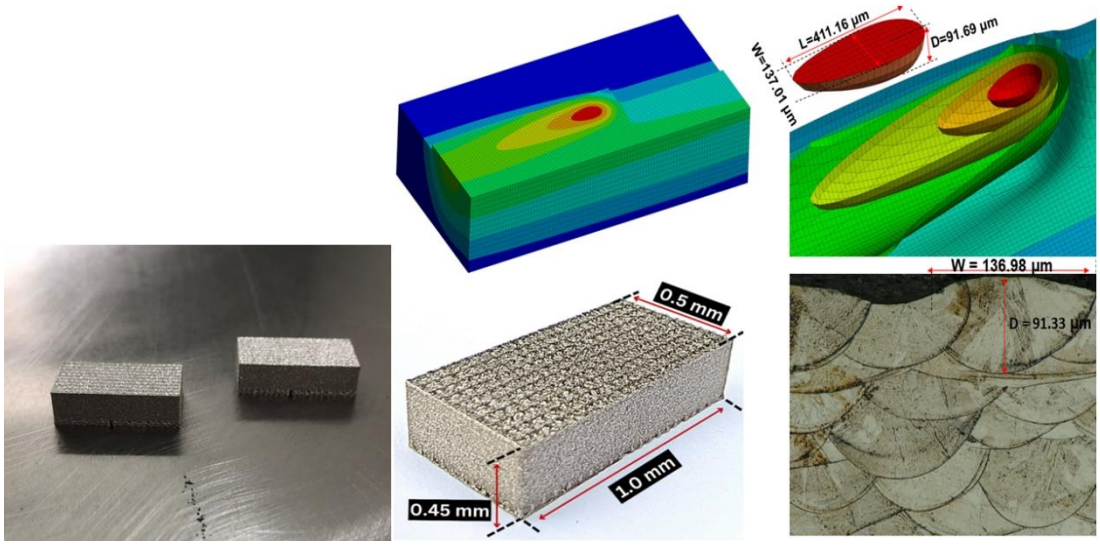

Figure 4.12. a). 3D printed geometry with substrate

The experimental data obtained from the Farsoon FS421M 3D metal printer was compared to the simulated data obtained using the developed numerical model. The evaluation of experimental and simulated data revealed that the model was capable of precisely forecasting the measurement of the melt pool. The validation of the numerical model using experimental data enhances the reliability of the model and its ability to predict the melt pool size accurately. The validated model can be used to optimize the process parameters of the 3D metal printing process, which can ultimately result in the production of high-quality products.

4.5.1 Variation in melt pool with process parameters:

The melt pool's width and depth profiles for optimal process parameters in SS316L SLM are presented in Figure 4.13, This data is helpful for predicting the size of the melt pool by adjusting the process parameters. The recommended parameters consist of a scanning speed ranging from 950-1250 mm/s, laser power between 180-240 W, a laser beam radius of 70.0-85.0 µm, a hatch spacing between 77.50-85.0 µm, and a layer thickness of 30.0 µm.

According to experimental results, the average width of the melt pool is approximately 138.91 µm, with a deviation of 1.88% from the numerical predictions. Additionally, the average depth of the melt pool is about 92.19 µm, with a deviation of 1.49% from both numerical and experimental measurements. Moreover, the average length of the melt pool is 342.10 µm, with a 2.12% discrepancy from prior and current numerical and experimental findings.

These results suggest that adjusting the process parameters can result in accurate estimations of the melt pool size. This data can be useful for optimizing the SLM process to produce high-quality parts with precise dimensions.

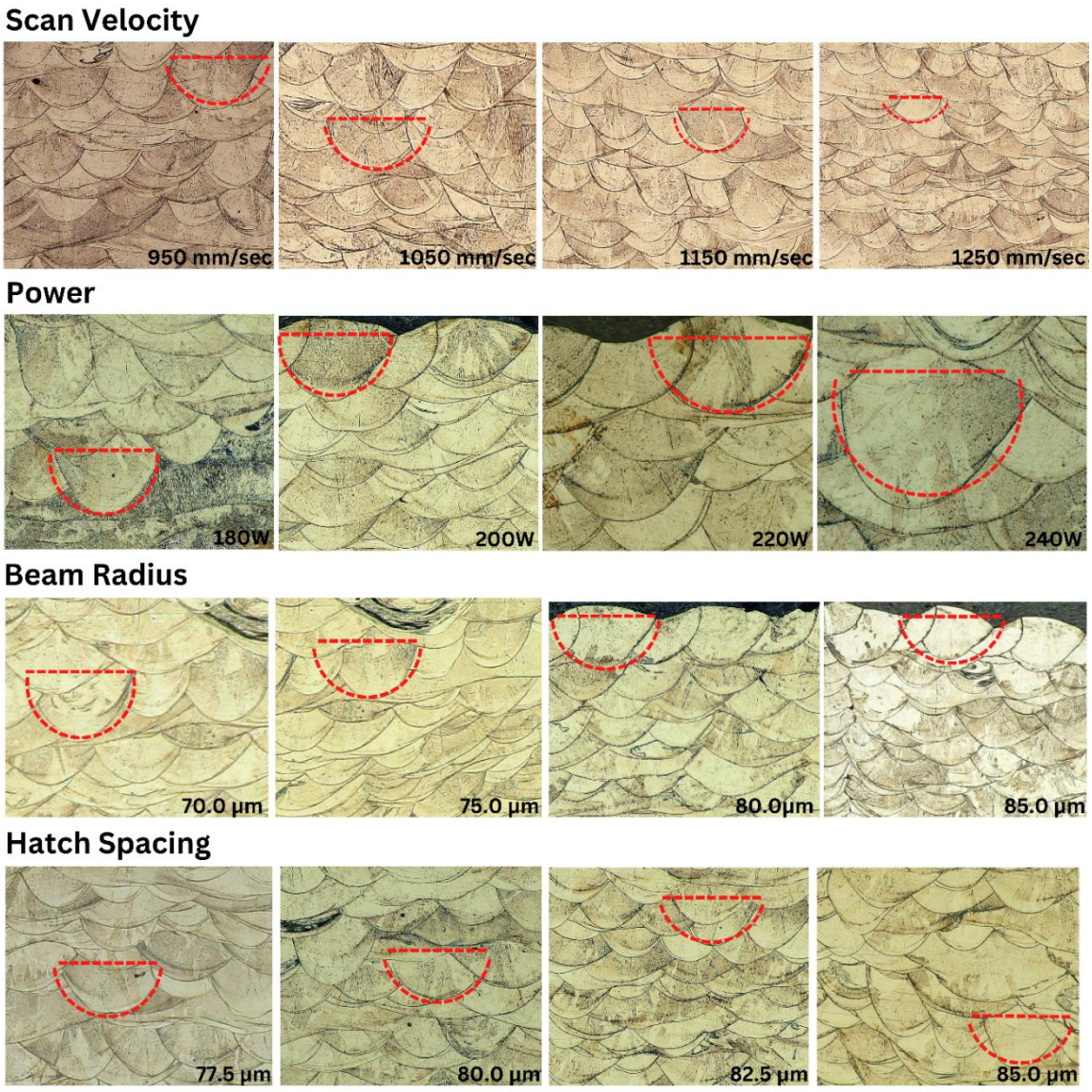

Figure 4.13. Experiment based Melt Pool dimensions measured with varying process parameters

Table 4.2. displays the melt pool dimensions obtained as a result of computations and experimental methods for different sets of process variables. The melt pool size was determined by analysing thermal distribution plots obtained during the laser scanning process. The melt pool length was measured along Y-axis along the laser scanning path, the width was measured along the X-axis. Similarly, the depth was also measured along the Z-axis, starting from the powder surface and reaching the molten depth within the powder bed. Conversely, the experimental measurements were obtained using a high-resolution optical microscope fabricated by OLYMPUS CORPORATION.

Table 4.2. Comparative analysis of numerical and experimentally measured Melt Pool dimensions with varying process parameters

Exp No.	Scan Speed (mm/sec)	Power (W)	Beam Radius (µm)	Hatch Spacing (µm)	Simulated Melt Pool Dimensions (µm)			Experimental Melt Pool Dimensions (µm)			% Error w.r.t Simulation Results		
					L	W	D	L	W	D	L	W	D
1	950	220	80	77.5	281.03	146.85	108.11	276.51	143.67	107.51	1.61	2.17	0.55
2	1050	220	80	77.5	348.99	143.65	94.77	340.14	140.52	93.36	2.54	2.18	1.49
3	1150	220	80	77.5	411.16	137.01	91.69	404.09	136.98	91.33	1.72	0.02	0.39
4	1250	220	80	77.5	443.60	133.84	82.07	432.90	132.86	80.85	2.41	0.73	1.49
5	1050	180	80	77.5	291.14	132.99	72.69	286.92	131.02	70.61	1.45	1.48	2.86
6	1050	200	80	77.5	318.99	137.05	86.04	314.14	133.02	83.76	1.52	2.94	2.65
7	1050	220	80	77.5	348.99	143.65	94.77	340.14	140.52	93.36	2.54	2.18	1.49
8	1050	240	80	77.5	377.99	148.24	117.22	371.10	146.04	113.48	1.82	1.48	3.19
9	1050	220	70	77.5	267.66	141.71	97.26	263.27	138.6	96.82	1.64	2.19	0.45
10	1050	220	75	77.5	322.13	142.01	95.14	316.21	139.76	94.73	1.84	1.58	0.43
11	1050	220	80	77.5	348.99	143.65	94.77	340.14	140.52	93.36	2.54	2.18	1.49
12	1050	220	85	77.5	385.13	145.58	91.56	374.57	144.42	90.20	2.74	0.80	1.49
13	1050	220	80	77.5	348.99	143.65	94.77	340.14	140.52	93.36	2.54	2.18	1.49
14	1050	220	80	80.0	334.09	142.13	93.94	323.53	139.02	91.55	3.16	2.19	2.54
15	1050	220	80	82.5	328.03	141.73	92.10	324.59	138.63	90.73	1.05	2.19	1.49
16	1050	220	80	85.0	319.71	141.12	90.41	310.44	136.03	90.07	2.90	3.61	0.38

Chapter 5 Conclusions and Recommendations

5.1 Conclusions:

A computational model using 3D finite element analysis was created to predict the thermal gradient and melt pool dimensions in the SLM of SS316L. In this modelling method, the impact of laser penetration depth on the characteristics of the melt pool was taken into account in a 15-layer, 6-track 3D Gaussian heat source model with varying process parameters such as Laser Power, Scan Speed, Beam Radius, and Hatch Spacing. However, particle size distribution was not included in this model. To validate the proposed heat source model, numerical and experimental data from previous studies were used, and additional experiments were conducted for further verification. The model's outcomes corresponded exceptionally well with the experimental findings, and the temperature distribution of each track and the dimensions of the melt pool, encompassing its width, depth, and length, were scrutinized and assessed.

1. The maximum temperature of the melt pool exhibited an increasing trend from Layer 1 to Layer 15, which was due to the accumulation of heat in the underlying layers and the growth of the melt pool. Specifically, the first ten deposition layers caused a temperature rise of 40-50°C, after which the temperature increase reduced to 2-5°C for the subsequent layers. As a result, there was only a minor increase of 0.5-1.5 µm in the average melt pool dimensions, indicating that the process had achieved steady-state conditions after the 10th layer and beyond.

2. As the successive tracks overlapped, there was an increase of 20-30 °C in the intertrack temperature, leading to an increase in the melt pool dimensions. The dimensions continued to increase until the process reached a steady state at 3rd and subsequent tracks. A uniform average dimensional fluctuation of 0.2-0.5 µm was detected for each track within a single layer.

3. The study evaluated how varying scanning velocities (950-1250mm/sec) affected the melt pool dimensions i.e., length, width, and depth. The findings indicated that as the scanning velocity increased, the length of the melt pool significantly grew, while its width and depth decreased. The outcomes exhibited an inverse correlation between the scanning velocity and the width and depth of the melt pool.

4. A minor elevation in laser power (180W to 240W) led to a substantial increase in the maximum temperature and depth of the melt pool, while the length and width of the pool remained relatively unaltered.

5. There was a direct relationship between the thermal gradient in the melt pool and the radius of the laser beam. Increasing the beam radius (from 70.0 µm to 85.0 µm) resulted in an expansion of the melt pool's dimensions (length and width), while the depth of the pool decreased due to a drop in the intensity of the laser beam.

6. The study found that increasing the hatch spacing from 77.5 µm to 85.0 µm resulted in a decrease in the thermal gradient at all levels. Consequently, the dimensions of the melt pool decreased due to greater heat accumulation in the tracks, causing track overlap.

The research indicated that the finite element model (FEM) produced precise outcomes, with the average melt pool dimensions obtained through experimentation exhibiting close similarity to the model. Upon analysing each variable, it was discovered that the FEM model had errors of 1.88%, 1.49%, and 2.12% in relation to the experimental measurements for the average length, width, and depth of the melt pool, respectively. Additionally, the temperature distribution in each track and the characteristics of the melt pool, including its width, length, and depth, were assessed and compared.

5.2 Recommendations:

There are several ways to expand and improve this study. However, it is necessary to conduct further research to verify the proposed model's performance by exploring a broader range of process parameters and metal alloys. Furthermore, it is essential to conduct in-depth experimental investigations into the extent of intense heating and the transition between melting modes. The effects of other process parameters, such as layer thickness, scanning pattern, and material feed rate for multiple-track cases, also need to be examined. Consequently, the proposed model can serve as a tool to estimate the process window and the melt pool's characteristics. In summary, this section highlights the potential for future studies.

1. Multiple thermal conductivities could be used in this study to enhance the model's precision across various energy density ranges, although a single thermal conductivity was employed.

2. While some of the processing parameters were fixed in this study for SLM fabrication, future research should consider altering various parameters such as scanning pattern, material feed rate, and layer thickness to produce parts with varying levels of densification and porosity.

3. The main objective of this dissertation was to examine the correlation between process parameters and melt pool geometry, as well as other process outcomes. Understanding the impact of process parameters can help prevent porosity formation and achieve the desired microstructure or other desired results. Although this study has made significant progress in understanding the effects of laser power, scan velocity, laser beam radius, and hatch spacing, there is still potential for further research and development.

4. Another potential avenue for future research is to measure and establish a correlation between the cooling rates and microstructure of the manufactured parts in each location while concurrently observing the temperature gradient

for the same location. This data may provide valuable insights into the solidification process and facilitate improvements in part quality.

5. The FEM model created in this research can be utilized to analyse various alloy systems by modifying their material properties. This approach could lead to faster characterization of newly discovered alloys.

REFERENCES:

[1] A. Riemer, S. Leuders, M. Thöne, H. Richard, T. Tröster, and T. Niendorf, "On the fatigue crack growth behavior in 316L stainless steel manufactured by selective laser melting," *Engineering Fracture Mechanics,* vol. 120, pp. 15-25, 2014.

[2] B. E. Carroll, T. A. Palmer, and A. M. Beese, "Anisotropic tensile behavior of Ti–6Al–4V components fabricated with directed energy deposition additive manufacturing," *Acta Materialia,* vol. 87, pp. 309-320, 2015.

[3] Y. Huang, L. Yang, X. Du, and Y. Yang, "Finite element analysis of thermal behavior of metal powder during selective laser melting," *International Journal of Thermal Sciences,* vol. 104, pp. 146-157, 2016.

[4] I. Yadroitsev, I. Yadroitsava, P. Bertrand, and I. Smurov, "Factor analysis of selective laser melting process parameters and geometrical characteristics of synthesized single tracks," *Rapid Prototyping Journal,* 2012.

[5] M. K. Gupta *et al.*, "Impact of layer rotation on micro-structure, grain size, surface integrity and mechanical behaviour of SLM Al-Si-10Mg alloy," *Journal of Materials Research and Technology,* vol. 9, no. 5, pp. 9506-9522, 2020.

[6] H. Ali, H. Ghadbeigi, F. Hosseinzadeh, J. Oliveira, and K. Mumtaz, "Effect of pre-emptive in situ parameter modification on residual stress distributions within selective laser-melted Ti6Al4V components," *The International Journal of Advanced Manufacturing Technology,* vol. 103, no. 9, pp. 4467-4479, 2019.

[7] C. Y. Yap *et al.*, "Review of selective laser melting: Materials and applications," *Applied physics reviews,* vol. 2, no. 4, p. 041101, 2015.

[8] A. T. Clare, P. R. Chalker, S. Davies, C. J. Sutcliffe, and S. Tsopanos, "Selective laser melting of high aspect ratio 3D nickel–titanium structures two way trained for MEMS applications," *International Journal of Mechanics and Materials in Design,* vol. 4, no. 2, pp. 181-187, 2008.

[9] M. Wong, S. Tsopanos, C. J. Sutcliffe, and I. Owen, "Selective laser melting of heat transfer devices," *Rapid Prototyping Journal,* 2007.

[10] B. Vandenbroucke and J. P. Kruth, "Selective laser melting of biocompatible metals for rapid manufacturing of medical parts," *Rapid Prototyping Journal,* 2007.

[11] P. Rochus, J.-Y. Plesseria, M. Van Elsen, J.-P. Kruth, R. Carrus, and T. Dormal, "New applications of rapid prototyping and rapid manufacturing (RP/RM) technologies for space instrumentation," *Acta Astronautica,* vol. 61, no. 1-6, pp. 352-359, 2007.

[12] D. A. Hollander *et al.*, "Structural, mechanical and in vitro characterization of individually structured Ti–6Al–4V produced by direct laser forming," *Biomaterials,* vol. 27, no. 7, pp. 955-963, 2006.

[13] A. Leicht, M. Rashidi, U. Klement, and E. Hryha, "Effect of process parameters on the microstructure, tensile strength and productivity of 316L parts produced by selective laser melting," *Materials Characterization,* vol. 159, p. 110016, 2020.

[14] M. Schmidt *et al.*, "Laser based additive manufacturing in industry and academia," *Cirp Annals,* vol. 66, no. 2, pp. 561-583, 2017.

[15] N. Khanna, S. Mistry, R. R. Rashid, and M. K. Gupta, "Investigations on density and surface roughness characteristics during selective laser sintering of Invar-36 alloy," *Materials Research Express,* vol. 6, no. 8, p. 086541, 2019.

[16] Z. Xiong, S. Liu, S. Li, Y. Shi, Y. Yang, and R. Misra, "Role of melt pool boundary condition in determining the mechanical properties of selective laser melting AlSi10Mg alloy," *Materials Science and Engineering: A,* vol. 740, pp. 148-156, 2019.

[17] A. Hussein, L. Hao, C. Yan, and R. Everson, "Finite element simulation of the temperature and stress fields in single layers built without-support in selective laser melting," *Materials & Design (1980-2015),* vol. 52, pp. 638-647, 2013.
[18] E. R. Denlinger, M. Gouge, J. Irwin, and P. Michaleris, "Thermomechanical model development and in situ experimental validation of the Laser Powder-Bed Fusion process," *Additive Manufacturing,* vol. 16, pp. 73-80, 2017.
[19] T. I. Zohdi, *Modeling and simulation of functionalized materials for additive manufacturing and 3d printing: continuous and discrete media: continuum and discrete element methods*. Springer, 2017.
[20] A. Alghamdi, D. Downing, M. McMillan, M. Brandt, M. Qian, and M. Leary, "Experimental and numerical assessment of surface roughness for Ti6Al4V lattice elements in selective laser melting," *The International Journal of Advanced Manufacturing Technology,* vol. 105, no. 1, pp. 1275-1293, 2019.
[21] H.-Z. Jiang *et al.*, "Factor analysis of selective laser melting process parameters with normalised quantities and Taguchi method," *Optics & Laser Technology,* vol. 119, p. 105592, 2019.
[22] J. D. Williams and C. R. Deckard, "Advances in modeling the effects of selected parameters on the SLS process," *Rapid Prototyping Journal,* vol. 4, no. 2, pp. 90-100, 1998.
[23] H. Gu, H. Gong, D. Pal, K. Rafi, T. Starr, and B. Stucker, "Influences of energy density on porosity and microstructure of selective laser melted 17-4PH stainless steel," in *2013 International Solid Freeform Fabrication Symposium*, 2013: University of Texas at Austin.
[24] A. Kudzal *et al.*, "Effect of scan pattern on the microstructure and mechanical properties of Powder Bed Fusion additive manufactured 17-4 stainless steel," *Materials & Design,* vol. 133, pp. 205-215, 2017.
[25] W. E. King *et al.*, "Observation of keyhole-mode laser melting in laser powder-bed fusion additive manufacturing," *Journal of Materials Processing Technology,* vol. 214, no. 12, pp. 2915-2925, 2014.
[26] K. Senthilkumaran, P. M. Pandey, and P. Rao, "New model for shrinkage compensation in selective laser sintering," *Virtual and Physical Prototyping,* vol. 4, no. 2, pp. 49-62, 2009.
[27] A. Simchi and H. Pohl, "Effects of laser sintering processing parameters on the microstructure and densification of iron powder," *Materials Science and Engineering: A,* vol. 359, no. 1-2, pp. 119-128, 2003.
[28] T. Furumoto *et al.*, "Permeability and strength of a porous metal structure fabricated by additive manufacturing," *Journal of Materials Processing Technology,* vol. 219, pp. 10-16, 2015.
[29] I. Yadroitsev, P. Krakhmalev, I. Yadroitsava, S. Johansson, and I. Smurov, "Energy input effect on morphology and microstructure of selective laser melting single track from metallic powder," *Journal of Materials Processing Technology,* vol. 213, no. 4, pp. 606-613, 2013.
[30] J. Liu *et al.*, "Effect of scanning speed on the microstructure and mechanical behavior of 316L stainless steel fabricated by selective laser melting," *Materials & Design,* vol. 186, p. 108355, 2020.
[31] I. Yadroitsev, A. Gusarov, I. Yadroitsava, and I. Smurov, "Single track formation in selective laser melting of metal powders," *Journal of Materials Processing Technology,* vol. 210, no. 12, pp. 1624-1631, 2010.

[32] C. Kusuma, S. H. Ahmed, A. Mian, and R. Srinivasan, "Effect of laser power and scan speed on melt pool characteristics of commercially pure titanium (CP-Ti)," *Journal of Materials Engineering and Performance,* vol. 26, no. 7, pp. 3560-3568, 2017.
[33] A. Gusarov, I. Yadroitsev, P. Bertrand, and I. Smurov, "Heat transfer modelling and stability analysis of selective laser melting," *Applied Surface Science,* vol. 254, no. 4, pp. 975-979, 2007.
[34] T. Childs, C. Hauser, and M. Badrossamay, "Selective laser sintering (melting) of stainless and tool steel powders: experiments and modelling," *Proceedings of the Institution of Mechanical Engineers, Part B: Journal of Engineering Manufacture,* vol. 219, no. 4, pp. 339-357, 2005.
[35] A. Grossmann, J. Felger, T. Froelich, J. Gosmann, and C. Mittelstedt, "Melt pool controlled selective laser melting for customised low-density lattice structures," *Materials & Design,* vol. 181, p. 108054, 2019.
[36] E. Yasa, J. Deckers, and J. P. Kruth, "The investigation of the influence of laser re-melting on density, surface quality and microstructure of selective laser melting parts," *Rapid Prototyping Journal,* 2011.
[37] X. Shi, S. Ma, C. Liu, and Q. Wu, "Parameter optimization for Ti-47Al-2Cr-2Nb in selective laser melting based on geometric characteristics of single scan tracks," *Optics & Laser Technology,* vol. 90, pp. 71-79, 2017.
[38] M. F. Zaeh and G. Branner, "Investigations on residual stresses and deformations in selective laser melting," *Production Engineering,* vol. 4, no. 1, pp. 35-45, 2010.
[39] K.-H. Leitz, P. Singer, A. Plankensteiner, B. Tabernig, H. Kestler, and L. Sigl, "Multi-physical simulation of selective laser melting," *Metal Powder Report,* vol. 72, no. 5, pp. 331-338, 2017.
[40] D. Zhang, P. Zhang, Z. Liu, Z. Feng, C. Wang, and Y. Guo, "Thermofluid field of molten pool and its effects during selective laser melting (SLM) of Inconel 718 alloy," *Additive Manufacturing,* vol. 21, pp. 567-578, 2018.
[41] Z. Li, R. Xu, Z. Zhang, and I. Kucukkoc, "The influence of scan length on fabricating thin-walled components in selective laser melting," *International Journal of Machine Tools and Manufacture,* vol. 126, pp. 1-12, 2018.
[42] M. Matsumoto, M. Shiomi, K. Osakada, and F. Abe, "Finite element analysis of single layer forming on metallic powder bed in rapid prototyping by selective laser processing," *International Journal of Machine Tools and Manufacture,* vol. 42, no. 1, pp. 61-67, 2002.
[43] Z. Luo and Y. Zhao, "Numerical simulation of part-level temperature fields during selective laser melting of stainless steel 316L," *The International Journal of Advanced Manufacturing Technology,* vol. 104, no. 5, pp. 1615-1635, 2019.
[44] L. Ma and H. Bin, "Temperature and stress analysis and simulation in fractal scanning-based laser sintering," *The International Journal of Advanced Manufacturing Technology,* vol. 34, no. 9, pp. 898-903, 2007.
[45] A. Nickel, D. Barnett, and F. Prinz, "Thermal stresses and deposition patterns in layered manufacturing," *Materials Science and Engineering: A,* vol. 317, no. 1-2, pp. 59-64, 2001.
[46] A. Artinov, M. Bachmann, and M. Rethmeier, "Equivalent heat source approach in a 3D transient heat transfer simulation of full-penetration high power laser beam welding of thick metal plates," *International Journal of Heat and Mass Transfer,* vol. 122, pp. 1003-1013, 2018.
[47] S. A. Khairallah, A. T. Anderson, A. Rubenchik, and W. E. King, "Laser powder-bed fusion additive manufacturing: Physics of complex melt flow and formation

mechanisms of pores, spatter, and denudation zones," *Acta Materialia,* vol. 108, pp. 36-45, 2016.
[48] W. Yan *et al.*, "Multi-physics modeling of single/multiple-track defect mechanisms in electron beam selective melting," *Acta Materialia,* vol. 134, pp. 324-333, 2017.
[49] A. Foroozmehr, M. Badrossamay, E. Foroozmehr, and S. i. Golabi, "Finite element simulation of selective laser melting process considering optical penetration depth of laser in powder bed," *Materials & Design,* vol. 89, pp. 255-263, 2016.
[50] J. Yin, H. Zhu, L. Ke, W. Lei, C. Dai, and D. Zuo, "Simulation of temperature distribution in single metallic powder layer for laser micro-sintering," *Computational Materials Science,* vol. 53, no. 1, pp. 333-339, 2012.
[51] A. K. Ibraheem, B. Derby, and P. J. Withers, "Thermal and residual stress modelling of the selective laser sintering process," *MRS Online Proceedings Library (OPL),* vol. 758, 2002.
[52] C. Shuai, P. Feng, C. Gao, Y. Zhou, and S. Peng, "Simulation of dynamic temperature field during selective laser sintering of ceramic powder," *Mathematical and Computer Modelling of Dynamical Systems,* vol. 19, no. 1, pp. 1-11, 2013.
[53] D. Gu, *Laser additive manufacturing of high-performance materials*. Springer, 2015.
[54] O. Diegel, A. Nordin, D. Motte, O. Diegel, A. Nordin, and D. Motte, "Additive manufacturing technologies," *A Practical Guide to Design for Additive Manufacturing,* pp. 19-39, 2019.
[55] Y. M. Wang *et al.*, "Additively manufactured hierarchical stainless steels with high strength and ductility," *Nature materials,* vol. 17, no. 1, pp. 63-71, 2018.
[56] M. S. F. de Lima and S. Sankaré, "Microstructure and mechanical behavior of laser additive manufactured AISI 316 stainless steel stringers," *Materials & Design,* vol. 55, pp. 526-532, 2014.
[57] G. Miranda *et al.*, "Predictive models for physical and mechanical properties of 316L stainless steel produced by selective laser melting," *Materials Science and Engineering: A,* vol. 657, pp. 43-56, 2016.
[58] P. Hanzl, M. Zetek, T. Bakša, and T. Kroupa, "The influence of processing parameters on the mechanical properties of SLM parts," *Procedia Engineering,* vol. 100, pp. 1405-1413, 2015.
[59] Q. Wei *et al.*, "Selective laser melting of stainless-steel/nano-hydroxyapatite composites for medical applications: Microstructure, element distribution, crack and mechanical properties," *Journal of Materials Processing Technology,* vol. 222, pp. 444-453, 2015.
[60] I. Tolosa, F. Garciandía, F. Zubiri, F. Zapirain, and A. Esnaola, "Study of mechanical properties of AISI 316 stainless steel processed by "selective laser melting", following different manufacturing strategies," *The International Journal of Advanced Manufacturing Technology,* vol. 51, pp. 639-647, 2010.
[61] Z. Sun, X. Tan, S. B. Tor, and C. K. Chua, "Simultaneously enhanced strength and ductility for 3D-printed stainless steel 316L by selective laser melting," *NPG Asia Materials,* vol. 10, no. 4, pp. 127-136, 2018.
[62] S.-h. Sun, T. Ishimoto, K. Hagihara, Y. Tsutsumi, T. Hanawa, and T. Nakano, "Excellent mechanical and corrosion properties of austenitic stainless steel with a unique crystallographic lamellar microstructure via selective laser melting," *Scripta Materialia,* vol. 159, pp. 89-93, 2019.
[63] S.-H. Sun, K. Hagihara, and T. Nakano, "Effect of scanning strategy on texture formation in Ni-25 at.% Mo alloys fabricated by selective laser melting," *Materials & Design,* vol. 140, pp. 307-316, 2018.

[64] M. L. Montero-Sistiaga, M. Godino-Martinez, K. Boschmans, J.-P. Kruth, J. Van Humbeeck, and K. Vanmeensel, "Microstructure evolution of 316L produced by HP-SLM (high power selective laser melting)," *Additive Manufacturing,* vol. 23, pp. 402-410, 2018.
[65] B. AlMangour, D. Grzesiak, and J.-M. Yang, "Scanning strategies for texture and anisotropy tailoring during selective laser melting of TiC/316L stainless steel nanocomposites," *Journal of Alloys and Compounds,* vol. 728, pp. 424-435, 2017.
[66] J. Suryawanshi, K. Prashanth, and U. Ramamurty, "Mechanical behavior of selective laser melted 316L stainless steel," *Materials Science and Engineering: A,* vol. 696, pp. 113-121, 2017.
[67] X. Zhou *et al.*, "Textures formed in a CoCrMo alloy by selective laser melting," *Journal of Alloys and Compounds,* vol. 631, pp. 153-164, 2015.
[68] H. Ali, H. Ghadbeigi, and K. Mumtaz, "Laser Melted Ti6Al4V, Materials Science & Engineering A," 2017.
[69] J. Antero, "Designing for Additive Manufacturing," 2019.
[70] J. L. Bartlett and X. Li, "An overview of residual stresses in metal powder bed fusion," *Additive Manufacturing,* vol. 27, pp. 131-149, 2019.
[71] I. Koutiri, E. Pessard, P. Peyre, O. Amlou, and T. De Terris, "Influence of SLM process parameters on the surface finish, porosity rate and fatigue behavior of as-built Inconel 625 parts," *Journal of Materials Processing Technology,* vol. 255, pp. 536-546, 2018.
[72] C. Pauzon, E. Hryha, P. Forêt, and L. Nyborg, "Effect of argon and nitrogen atmospheres on the properties of stainless steel 316 L parts produced by laser-powder bed fusion," *Materials & Design,* vol. 179, p. 107873, 2019.
[73] L.-E. Loh *et al.*, "Numerical investigation and an effective modelling on the Selective Laser Melting (SLM) process with aluminium alloy 6061," *International Journal of Heat and Mass Transfer,* vol. 80, pp. 288-300, 2015.
[74] P. S. Cook and A. B. Murphy, "Simulation of melt pool behaviour during additive manufacturing: Underlying physics and progress," *Additive Manufacturing,* vol. 31, p. 100909, 2020.
[75] L. E. Criales, Y. M. Arısoy, and T. Özel, "A sensitivity analysis study on the material properties and process parameters for selective laser melting of Inconel 625," in *International Manufacturing Science and Engineering Conference*, 2015, vol. 56826: American Society of Mechanical Engineers, p. V001T02A062.
[76] Z. Zhang *et al.*, "3-Dimensional heat transfer modeling for laser powder-bed fusion additive manufacturing with volumetric heat sources based on varied thermal conductivity and absorptivity," *Optics & Laser Technology,* vol. 109, pp. 297-312, 2019.
[77] J.-R. Zhuang, Y.-T. Lee, W.-H. Hsieh, and A.-S. Yang, "Determination of melt pool dimensions using DOE-FEM and RSM with process window during SLM of Ti6Al4V powder," *Optics & Laser Technology,* vol. 103, pp. 59-76, 2018.
[78] F. Verhaeghe, T. Craeghs, J. Heulens, and L. Pandelaers, "A pragmatic model for selective laser melting with evaporation," *Acta Materialia,* vol. 57, no. 20, pp. 6006-6012, 2009.
[79] D. Sowdari and P. Majumdar, "Finite element analysis of laser irradiated metal heating and melting processes," *Optics & Laser Technology,* vol. 42, no. 6, pp. 855-865, 2010.
[80] C. Chen *et al.*, "The effect of process parameters on the residual stress of selective laser melted Inconel 718 thin-walled part," *Rapid Prototyping Journal,* 2019.

[81] T. Larimian, M. Kannan, D. Grzesiak, B. AlMangour, and T. Borkar, "Effect of energy density and scanning strategy on densification, microstructure and mechanical properties of 316L stainless steel processed via selective laser melting," *Materials Science and Engineering: A,* vol. 770, p. 138455, 2020.
[82] A.-M. Bandar, R. Mongrain, E. Irissou, and S. Yue, "Improving the strength and corrosion resistance of 316L stainless steel for biomedical applications using cold spray," *Surface and Coatings Technology,* vol. 216, pp. 297-307, 2013.
[83] X. Chen, J. Lu, L. Lu, and K. Lu, "Tensile properties of a nanocrystalline 316L austenitic stainless steel," *Scripta materialia,* vol. 52, no. 10, pp. 1039-1044, 2005.
[84] I. Gotman, "Characteristics of metals used in implants," *Journal of endourology,* vol. 11, no. 6, pp. 383-389, 1997.
[85] Y. Kim, Y. Kim, D. Kim, S. Kim, W. Nam, and H. Choe, "Effects of hydrogen diffusion on the mechanical properties of austenite 316L steel at ambient temperature," *Materials transactions,* vol. 52, no. 3, pp. 507-513, 2011.
[86] W. M. Tucho, V. H. Lysne, H. Austbø, A. Sjolyst-Kverneland, and V. Hansen, "Investigation of effects of process parameters on microstructure and hardness of SLM manufactured SS316L," *Journal of Alloys and Compounds,* vol. 740, pp. 910-925, 2018.
[87] W. Huang and Y. Zhang, "Finite element simulation of thermal behavior in single-track multiple-layers thin wall without-support during selective laser melting," *Journal of Manufacturing Processes,* vol. 42, pp. 139-148, 2019.
[88] S. Liu, J. Zhu, H. Zhu, J. Yin, C. Chen, and X. Zeng, "Effect of the track length and track number on the evolution of the molten pool characteristics of SLMed Al alloy: Numerical and experimental study," *Optics & Laser Technology,* vol. 123, p. 105924, 2020.
[89] Y. Liu, J. Zhang, and Z. Pang, "Numerical and experimental investigation into the subsequent thermal cycling during selective laser melting of multi-layer 316L stainless steel," *Optics & Laser Technology,* vol. 98, pp. 23-32, 2018.
[90] T. DebRoy *et al.*, "Additive manufacturing of metallic components–process, structure and properties," *Progress in Materials Science,* vol. 92, pp. 112-224, 2018.
[91] D. Dai and D. Gu, "Influence of thermodynamics within molten pool on migration and distribution state of reinforcement during selective laser melting of AlN/AlSi10Mg composites," *International Journal of Machine Tools and Manufacture,* vol. 100, pp. 14-24, 2016.
[92] X. Zhang, L. Chen, J. Zhou, and N. Ren, "Simulation and experimental studies on process parameters, microstructure and mechanical properties of selective laser melting of stainless steel 316L," *Journal of the Brazilian Society of Mechanical Sciences and Engineering,* vol. 42, no. 8, pp. 1-14, 2020.
[93] U. S. Bertoli, A. J. Wolfer, M. J. Matthews, J.-P. R. Delplanque, and J. M. Schoenung, "On the limitations of volumetric energy density as a design parameter for selective laser melting," *Materials & Design,* vol. 113, pp. 331-340, 2017.
[94] Z. Huang *et al.*, "A new heat source model for selective laser melting simulations based on energy distribution on the powder layer and the surface of substrate," *arXiv preprint arXiv:2106.03482,* 2021.
[95] N. Ahmed, I. Barsoum, G. Haidemenopoulos, and R. A. Al-Rub, "Process parameter selection and optimization of selective laser melting for 316L stainless steel: A review," *Journal of Manufacturing Processes,* vol. 75, pp. 415-434, 2022.
[96] M. Khorasani *et al.*, "On the role of process parameters on meltpool temperature and tensile properties of stainless steel 316L produced by powder bed fusion," *journal of materials research and technology,* vol. 12, pp. 2438-2452, 2021.

[97] T. Heeling, M. Cloots, and K. Wegener, "Melt pool simulation for the evaluation of process parameters in selective laser melting," *Additive Manufacturing,* vol. 14, pp. 116-125, 2017.
[98] H.-C. Tran and Y.-L. Lo, "Heat transfer simulations of selective laser melting process based on volumetric heat source with powder size consideration," *Journal of Materials Processing Technology,* vol. 255, pp. 411-425, 2018.
[99] A. Gusarov, I. Yadroitsev, P. Bertrand, and I. Smurov, "Model of radiation and heat transfer in laser-powder interaction zone at selective laser melting," *Journal of heat transfer,* vol. 131, no. 7, 2009.
[100] Y. Li, K. Zhou, P. Tan, S. B. Tor, C. K. Chua, and K. F. Leong, "Modeling temperature and residual stress fields in selective laser melting," *International Journal of Mechanical Sciences,* vol. 136, pp. 24-35, 2018.
[101] J. Trejos-Taborda, L. Reyes-Osorio, C. Garza, P. del Carmen Zambrano-Robledo, and O. Lopez-Botello, "Finite element modeling of melt pool dynamics in selective laser melting of 316L stainless steel," *The International Journal of Advanced Manufacturing Technology,* vol. 120, no. 5, pp. 3947-3961, 2022.
[102] K.-H. Lee and G. J. Yun, "A novel heat source model for analysis of melt Pool evolution in selective laser melting process," *Additive Manufacturing,* vol. 36, p. 101497, 2020.
[103] N. Hodge, R. Ferencz, and J. Solberg, "Implementation of a thermomechanical model for the simulation of selective laser melting," *Computational Mechanics,* vol. 54, no. 1, pp. 33-51, 2014.